1D Scramjet Model

by

Geoffrey Svensson

Submitted to the Department of Aeronautics and Astronautics
in partial fulfillment of the requirements for the degree of

Master of Science in Aeronautics and Astronautics

at the

MASSACHUSETTS INSTITUTE OF TECHNOLOGY

September 2020

Author .....
Department of Aeronautics and Astronautics
August 18, 2020

Certified by .....
Wesley L. Harris
C.S. Draper Professor of Aeronautics and Astronautics
Thesis Supervisor

Accepted by .....
Zoltán Spakovszky
Chairman, Department Committee on Graduate Theses

1D Scramjet Model

by

Geoffrey Svensson

Submitted to the Department of Aeronautics and Astronautics
on August 18, 2020, in partial fulfillment of the
requirements for the degree of
Master of Science in Aeronautics and Astronautics

Abstract

Renewed interest in hypersonic research has motivated a number of scientists to re-investigate the efficacy and performance of supersonic combustion ramjets, colloquially known as "scramjets". In this thesis, a 1-D scramjet model is proposed which shall be able to simulate separated flows within the isolator as well as the pressure distributions in a scramjet combustor. The goal is to divine the trends and sensitivities that are most significant in a given engine design, as well as provide a platform for further research into supersonic combustion. The model accurately predicts the stagnation and static quantities within a scramjet and can simulate the trends found in real life experiments. The 1D model gives significant physical insight to scramjet operation as it establishes key trade offs that scramjet analysis necessitate.

Thesis Supervisor: Wesley L. Harris
Title: C.S. Draper Professor of Aeronautics and Astronautics

Acknowledgments

I would first like to thank my advisor, Professor Harris, for his guidance and input on this project for these last few years. I would especially like to thank him for his support during this unprecedented pandemic of COVID-19, which has affected all of us in the research community.

I would also like to thank my colleagues in the Hypersonic Research Team as well as some of my friends outside of AeroAstro who have all contributed valuable insight to this project.

Lastly I would like to thank my parents and family, as their love and support have been especially important during this time of great uncertainty and upheaval. Crafting this thesis from the comfort of my home would not have been possible without them.

Contents

List of Figures

List of Tables

Chapter 1

Introduction

1.1 Background

Renewed interest in hypersonic research has motivated a number of scientists to re-investigate the efficacy and performance of supersonic combustion ramjets, colloquially known as "scramjets". A key advantage of a scramjet lies in its ability to maintain a relatively high specific impulse compared to rocket propulsion in the hypersonic flow regime - that is, where flight mach number exceeds 5.

With rocket propulsion reaching its theoretical limits on Isp, scramjets present a comparative advantage to rockets in several ways, such as longer range and a larger flight envelope for the vehicles in which they are integrated. In addition to higher Isp, scramjets are air-breathing engines, relieving the aircraft of having to carry its own oxidizer and the associated weight penalties. A whole host of theoretical vehicles have been imagined with these capabilities in mind, including Single Stage To Orbit (SSTO) aircraft and advanced missile systems.

A typical scramjet can be broken into four distinct regions: The inlet, isolator, combustor, and nozzle. A notable feature of the scramjet is that it contains no moving parts; its operation is very similar to that of a ramjet. The main difference to a ramjet is that the throughflow remains supersonic, including through the combustor, thus the primary challenge in scramjet design is managing the complexities of compressible, supersonic flow. Each station must accomplish its respective duty while

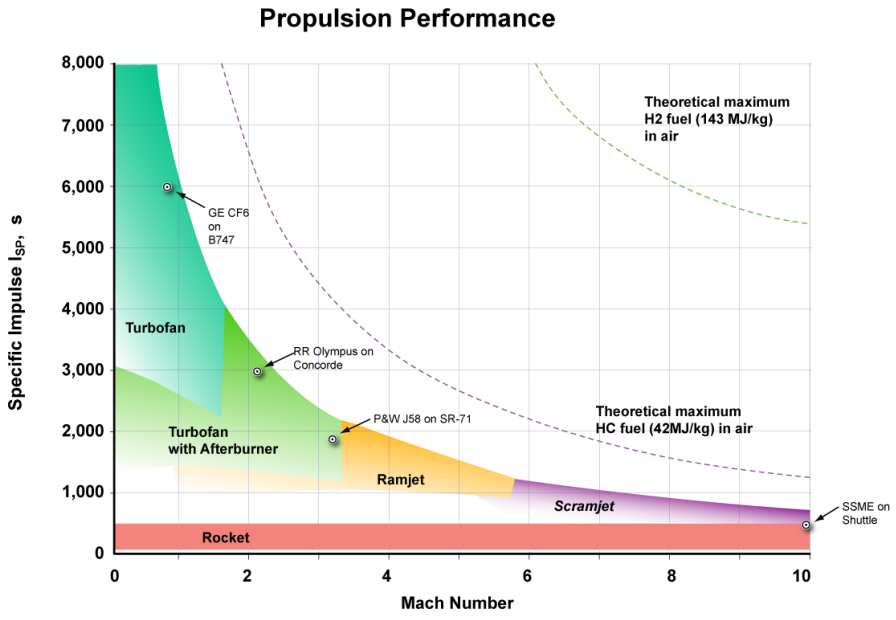

Figure 1-1: Isp versus Mach number for various propulsive systems [1]

keeping stagnation pressure losses to a minimum, which can be a difficult task in a high enthalpy flow. Naturally, engineers would like to predict the performance of a given scramjet design, so a model which analyzes the whole system or a particular component can be very useful.

1.2 Prior Work

Despite interest in scramjets waxing and waning periodically, significant advancements in our understanding have been made both on the theoretical and experimental fronts. In recent memory, one of the largest pushes in scramjet technology was the National Aerospace Plane (NASP), also known as the X-30, which was developed by NASA and the Department of Defense. It was envisioned as a single stage to orbit (SSTO) aircraft which would be powered by a hydrogen fueled scramjet. However, due to funding difficulties, the project was scrapped and no plane was ever built. Additionally, a system level analysis revealed that the concept was not feasible due to the energy requirements of leaving the atmosphere, further cementing its demise. The insights from its development were carried over to smaller scale unmanned ex-

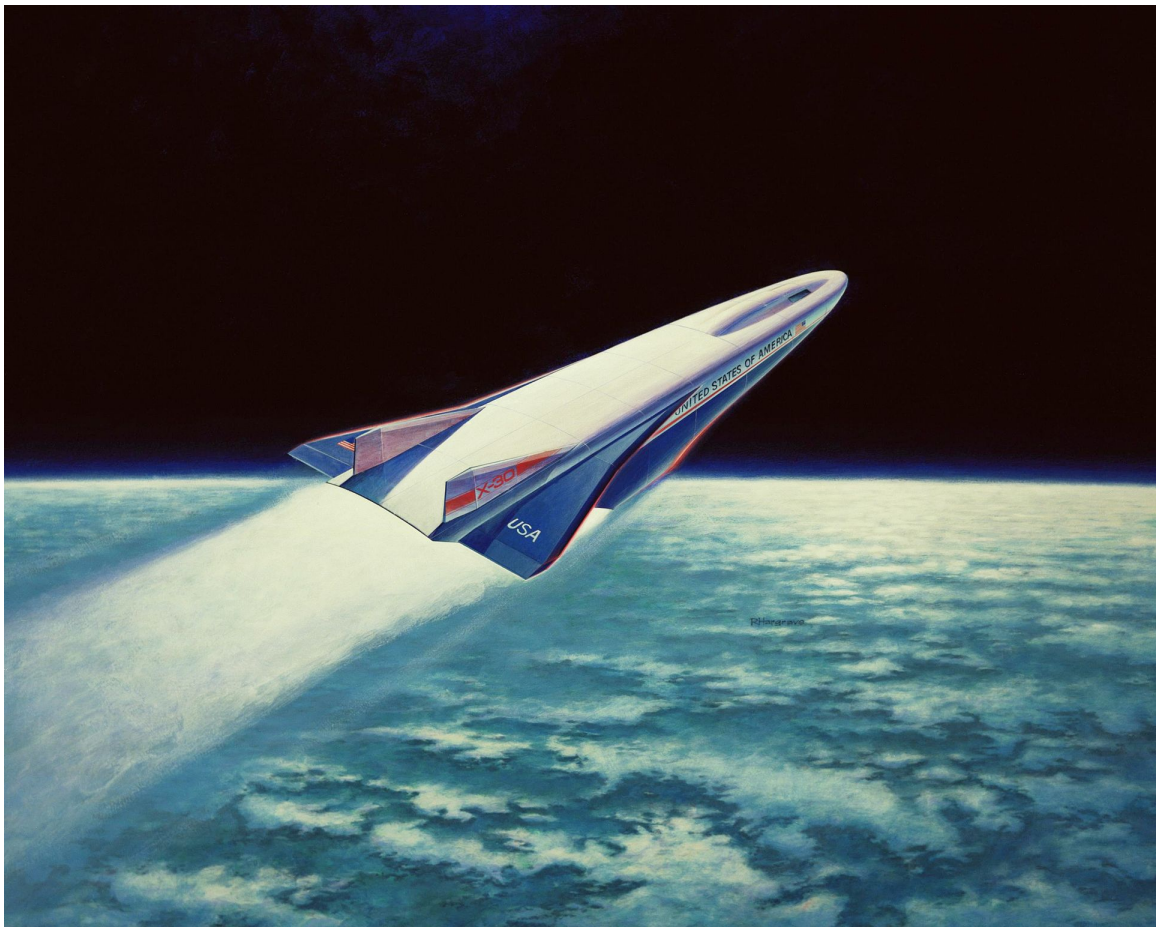

Figure 1-2: NASA's National Aerospace Plane [2]

perimental aircraft, however, such as the X-43 and X-51. The X-43 hit a record speed of Mach 9.68 at 112,000 feet in 2004, and in 2010, the X-51 successfully flew at Mach 5 for over 200 seconds, breaking the record for longest scramjet operation.[13] With plenty of examples of scramjets successfully working at flight conditions, researchers have renewed confidence in their potential.

1.3 Motivation

The purpose of the 1-D scramjet model is to evaluate the performance of each individual component as well as the overall system in the context of flight conditions. The model shall be able to simulate separated flows within the isolator as well as the pressure distributions in a scramjet combustor. The goal is to divine the trends and

sensitivities that are most significant in a given engine design, as well as provide a platform for further research into supersonic combustion. For each station, a variety of modeling techniques are offered with the intent to calculate the most important parameters regarding a propulsive system. A special emphasis will be given to the combustion of ethylene fuel, since its properties have certain advantages in scramjet engines which would be useful to quantify, such as its high volumetric energy density compared to hydrogen, its short ignition times compared to flow through time, and its relevance as an intermediary fuel in the decomposition of larger chained hydrocarbons such as JP7.

1.4 Thesis Outline

The Thesis is organized into 5 chapters, each dedicated to a specific part of the scramjet and the :

1. Chapter 1: Introduction

2. Chapter 2: Cycle analysis and general model assumptions, Here the general thermodynamic description of a scramjet will be given as well as some of the parameters needed to initialize the model

3. Chapter 3: Inlet modeling and comparison of different inlet types; this section shall be dedicated to approximating the stagnation quantities entering the isolator and combustor.

4. Chapter 4: Isolator Model and 1D Flow equations: this section will be dedicated to establishing the mathematics used to model compressible channel flow as well as the separated flow results in an isolator

5. Chapter 5: Here a discussion of fuel choice and chemical modeling will be explored, as well as results of the full scramjet model and how they compare to experimental results.

Chapter 2

Cycle Analysis and Initialization

2.1 Cycle Analysis

In order to lay the foundation for the subsequent analysis, it's worthwhile to investigate the underlying thermodynamics of a scramjet, which is described by the ideal Brayton cycle: Adiabatic Compression, constant pressure heat addition, adiabatic expansion, and constant pressure heat rejection. Referring to the diagram, each station on the scramjet represents an area where a thermodynamic process is carried out.

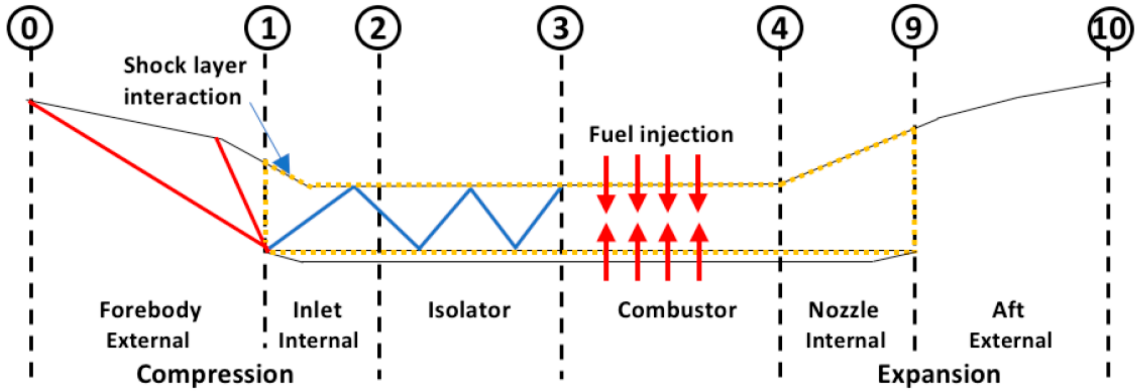

Figure 2-1: A generalized scramjet breakdown[3]

The breakdown of each station is as follows:

1. Station 0: This is the free stream condition and represents the incoming flow. The important values for this station are the flight Mach number M_0, stagnation

pressure P_0, and stagnation temperature T_0.

2. Stations 1-3: In the forebody of the scramjet are the "inlet" and isolator components of the engine. Pictured above is a design which uses a mixed inlet with both external and internal compression ramps as well as an internal isolator. The entire purpose of these sections is to slow the incoming air by a series of oblique shockwaves, thereby increasing the static pressure P and static temperature T while minimizing stagnation pressure loss. In addition to compressing the inlet flow, the isolator also serves as a threshold between the combustor and the upstream shockwaves, with the intent to dissociate any upstream influence of the supersonic combustion process. In normal operation, the internal flow is attached, however, if the combustor pressure rise is large enough to cause flow separation, a series of shock waves are created which can travel upstream and upset the carefully balanced oblique shock system of the inlet. Thus the isolator is intended to "contain" this flow separation and nullify the upstream influence.

3. Stations 3-4: In the heart of the scramjet lies the combustor, where fuel and air are ignited and heat is released, resulting in an increase in stagnation temperature T0 and a small decrease in stagnation pressure. Due to the complexity of supersonic combustion, it is the most difficult component to model and requires very careful consideration of input values, assumptions, and boundary conditions. Essential to its modeling are the time scales involved with the chemical kinetics and the flow through time of fluid.

4. Stations 4-10: In a similar manner to the inlet, with both internal and external sections, the nozzle accelerates the hot gas by expansion, thereby increasing the kinetic energy of the flow and decreasing its static pressure and static temperature. Ideally, a well designed nozzle will expand the gas such that its static pressure matches the ambient pressure of the atmosphere.

A cursory analysis of these stations, treating them as ideal, gives insight to the thermodynamic advantages of the scramjet engine. The Brayton cycle is best represented with a T-s diagram, with each station marked on the graph.

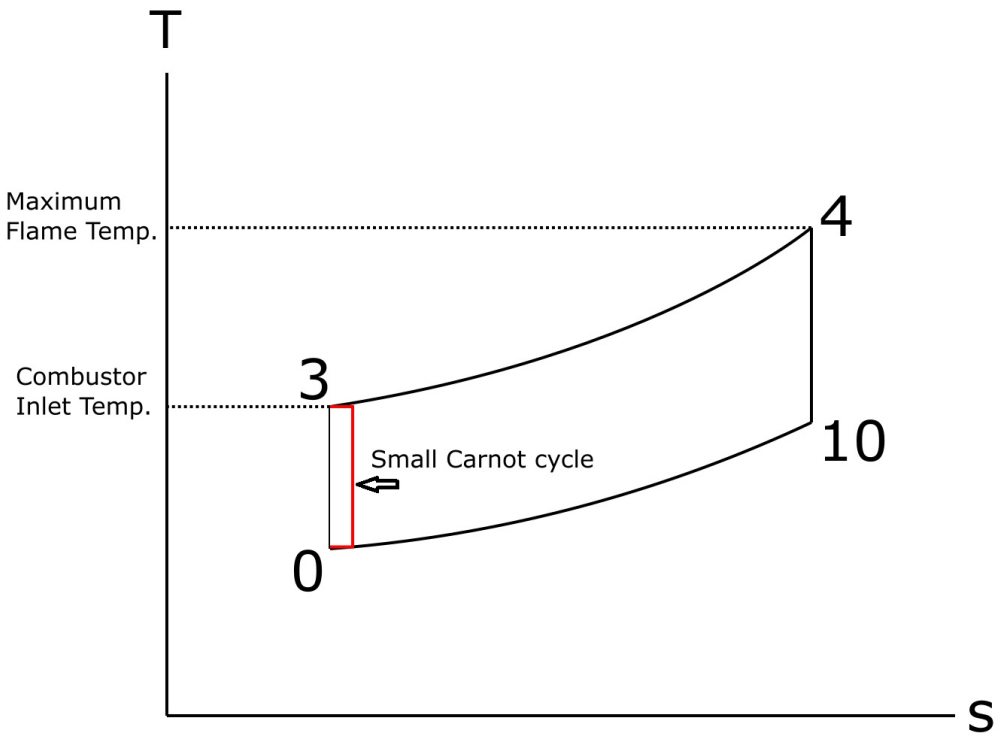

Figure 2-2: T-s Diagram of a Brayton cycle

It is possible to evaluate the thermal efficiency of a Brayton cycle by analyzing the incremental increases of temperature and entropy, which happen to represent a Carnot cycle in which isentropic compression, isothermal heat addition, and isentropic expanison all occur in sequence. By treating each incremental temperature increase as a small Carnot cycle and subsequently adding them together to form the whole cycle, we are able to derive that the thermal efficiency of the engine is:

$$\eta_t = 1 - \frac{T_0}{T_3} \tag{2.1}$$

From the First Law of Thermodynamics and the definition of the speed of sound in a fluid, we have the fundamental relationship between a fluid's stagnation temperature, static temperature and Mach number:

$$T_t = T\left(1 + \frac{\gamma - 1}{2} M^2\right) \tag{2.2}$$

Using these two expressions and substituting for each respective station, we are able to rearrange the equation such that we have an expression for the thermal efficiency in terms of the Mach numbers in the free stream and at the combustor inlet:

$$\eta_t = 1 - \frac{1 + \frac{\gamma-1}{2} M_3^2}{1 + \frac{\gamma-1}{2} M_0^2} \tag{2.3}$$

With this relation, we arrive at the first key non-dimensional parameter describing the scramjet, $\frac{M_3}{M_0}$, which is ultimately the designer's choice for tuning the thermal efficiency of the scramjet. Visualized, we can see directly how as Mach number increases, so does the thermal efficiency:

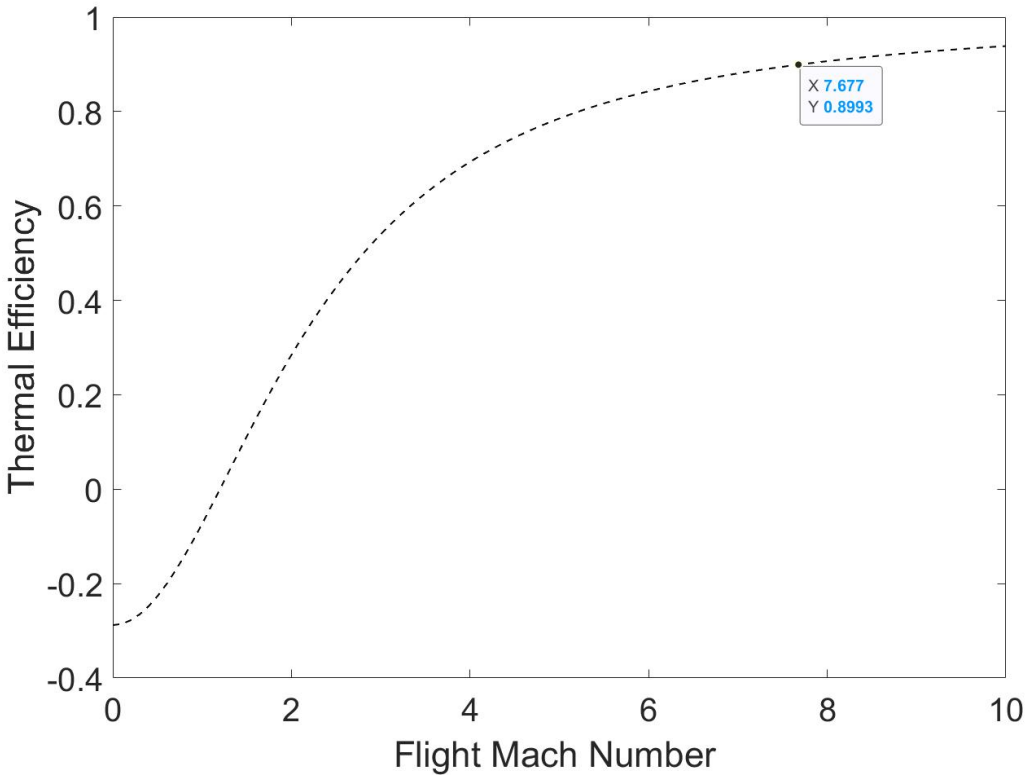

Figure 2-3: Thermal efficiency of a scramjet with $M_3 = 1.2$

Analyzing this figure, there are a few aspects to scramjet operation which are

revealed: Firstly, at flight Mach numbers less than 4, the thermal efficiency of the cycle remains low, which happens to be in the flight region where a ramjet with subsonic combustion is far better suited. A major problem with scramjets is getting them started, and some ideas suggest a "dual mode" whereby a ramjet accelerates to a high enough Mach number and crosses over to scramjet operation.[2] In this scheme, a combustor can operate with both subsonic and supersonic through flow, thereby adjusting the above curve to higher thermal efficiencies across the flight envelope and allowing for on the fly modification of $\frac{M_3}{M_0}$.

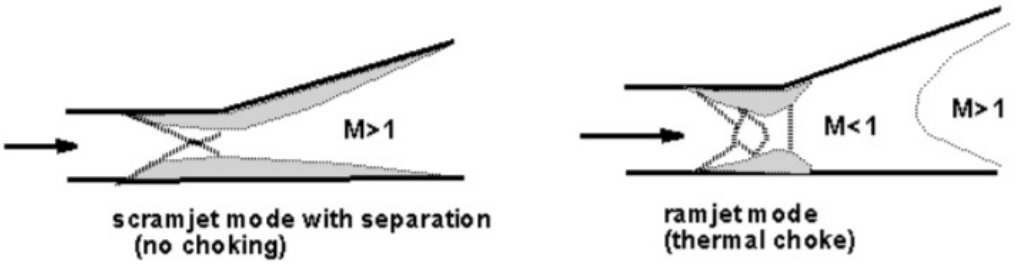

Figure 2-4: Illustration of scramjet vs. ramjet modes [4]

A certain level of complexity exists with these types of engines, so for the time being, the model will treat only scramjet operation only. Referring back to Figure 5-9, we see that in the hypersonic flow regime, $M_0 > 5$, the thermal efficiency starts to approach very high values, with efficiencies as high as $\eta_t = .9$. Therein lies the secret to the scramjet's capabilities, as relatively little heat addition is required from its fuel to produce useful thrust. Thus, the brief analysis above demonstrates the scramjet's strong potential in hypersonic propulsion.

2.1.1 Non-Ideal Cycle Analysis

Unfortunately the Scramjet is not immune to irreversibilites present in other propulsion systems, so it is worthwhile to comment on each respective station's shortcomings:

1. Stations 1-3: The inlet of a scramjet contains a series of oblique shockwaves,

which create unavoidable losses in the flow's stagnation pressure. These losses can be accounted by an increase in entropy s on the T-s diagram. In addition, the very high stagnation temperature of the flow is found in the boundary layers formed on the inlet's walls, which results in a heat transfer between the body of the aircraft and the high temperature gas. Similar losses occur in the isolator as well.

2. Stations 3-4: In order to combust air and fuel efficiently, mixing is required, which can lead to an increase in entropy and a loss in total pressure. Additionally, due to Rayleigh flow dynamics, there is an unavoidable loss in total pressure when combusting supersonically.

3. Stations 4-10: The losses occurring in the nozzle stem from a mismatch between the exit flow pressure and the atmospheric pressure, leading to expansion waves in the jet stream. Put another way, the expansion of the gas is not fully utilized, leading to a loss in efficiency.

Visualized, we can compare the ideal cycle to the more realistic cycle depicted on the T-s diagram: The essence of the 1-D model is to try to accurately capture these irreversibilities and their underlying physical mechanisms. With these phenomena quantified, one is able to see how the various components influence one another as well as establish reasonable expectations of scramjet performance.

2.2 Intialization

In order to initialize the model, it is necessary to establish the operating conditions under which the theoretical scramjet will be operating. Thus, the US Standard Atmosphere shall be used, and a flight Mach number in the hypersonic regime will be specified. With Mach number and altitude set, we are able to determine our inlet values: P_t, T_t, M_0, ρ.

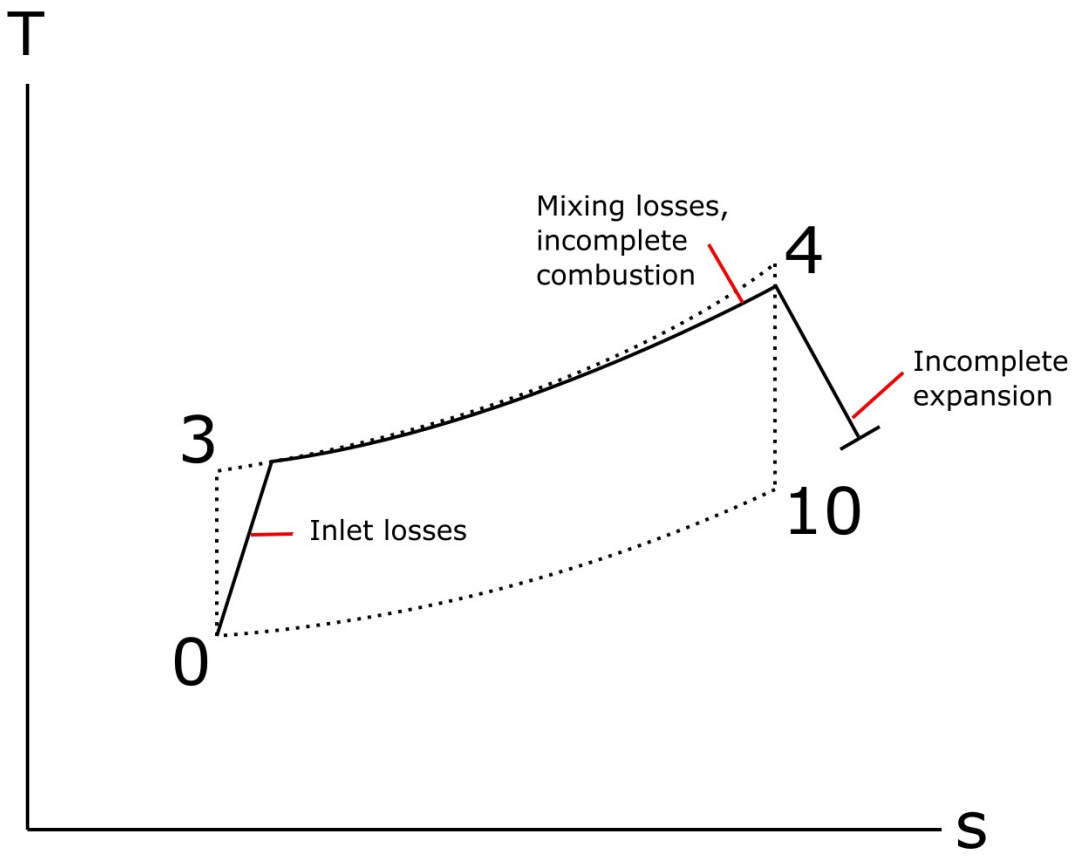

Figure 2-5: Ideal vs. non ideal scramjet

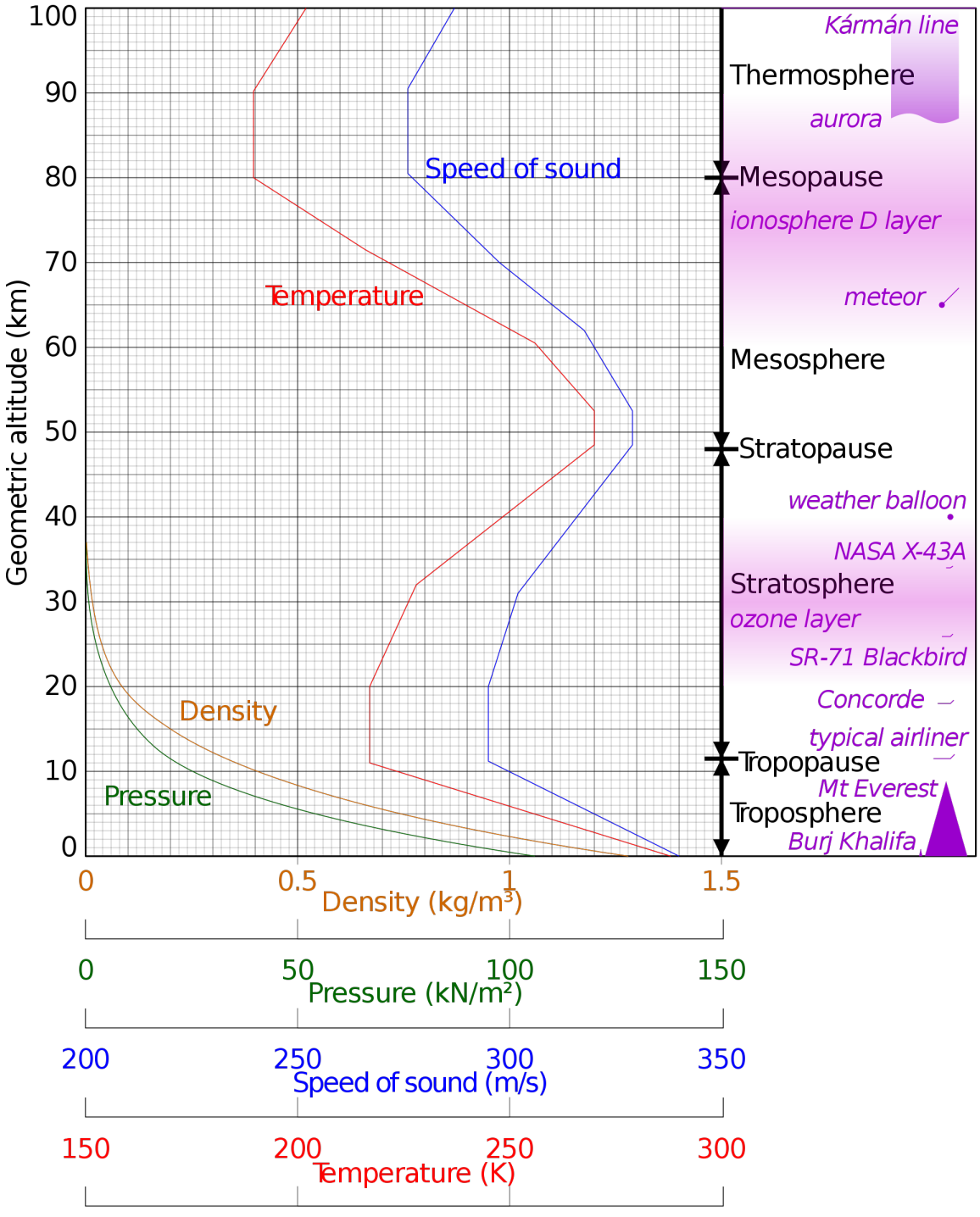

Figure 2-6: US Standard Atmosphere [5]

Chapter 3

Inlet Model

3.1 Overview

The inlet of a scramjet is the first point of contact for incoming flow to the engine and thus has the distinguished role of conditioning air for combustion. Not only must it compress the static pressure of the incoming air, but it has to do so while minimizing total pressure losses and remaining stable through various flight Mach numbers. In addition to keeping the flow's linear momentum, the inlet must also contend with heat transfer and cooling itself, as well as remaining supersonically "started" during unsteady combustion transients. These are complicated and in depth topics which scientists spend much effort researching and trying to model. In the case of this model, it shall be assumed that the engine is operating in a steady state, however it is worth mentioning that this steadiness is not always a given.

Several inlet designs for hypersonic airbreathing propulsion exist. The most common type is a single ramp style, where a chosen ramp angle creates a series oblique shockwaves which focus upon a single locus. Courtesy of [14] we have a useful figure to illustrate this design:

This design is relatively popular due to its simplicity, and is typically modeled using the Method of Characteristics to solve the accompanying Prandtl-Meyer expansion flow. However, other designs exist which can provide even better stagnation pressure recovery, such as the Busemann inlet or the Oswatitsch inlet. The essence

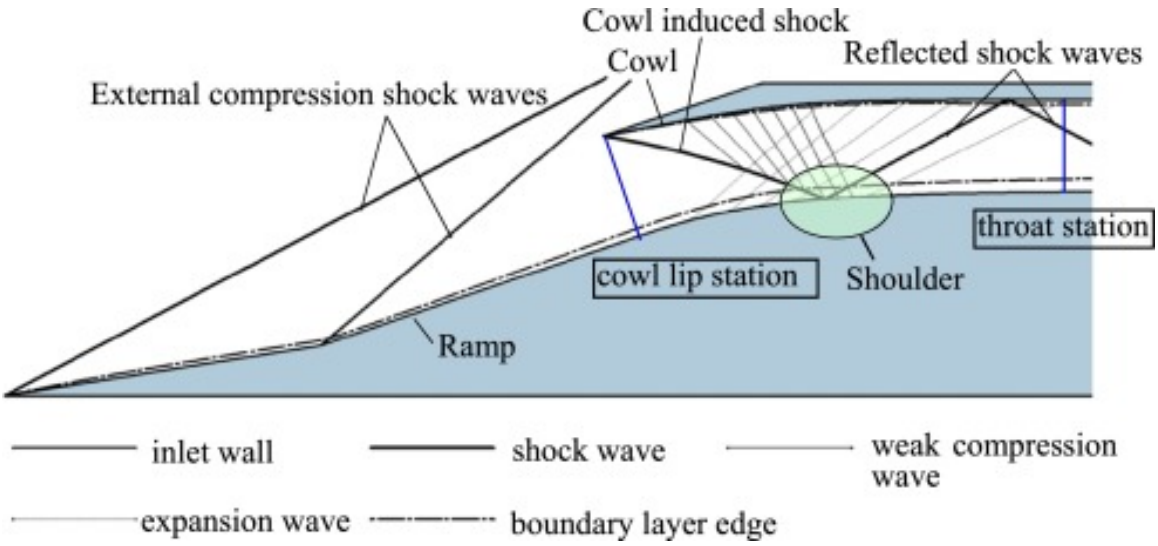

Figure 3-1: A single ramp style inlet

of these inlets is that they have a conical design which reduces the surface area on which boundary layers form for the same inlet area, thereby decreasing the viscous losses associated with them. Compared to a typical single ramp, rectangular inlet, these more advanced inlets are axisymmetric as well, which helps mitigate 3D flow effects. A cross section of these inlets is provided[14]:

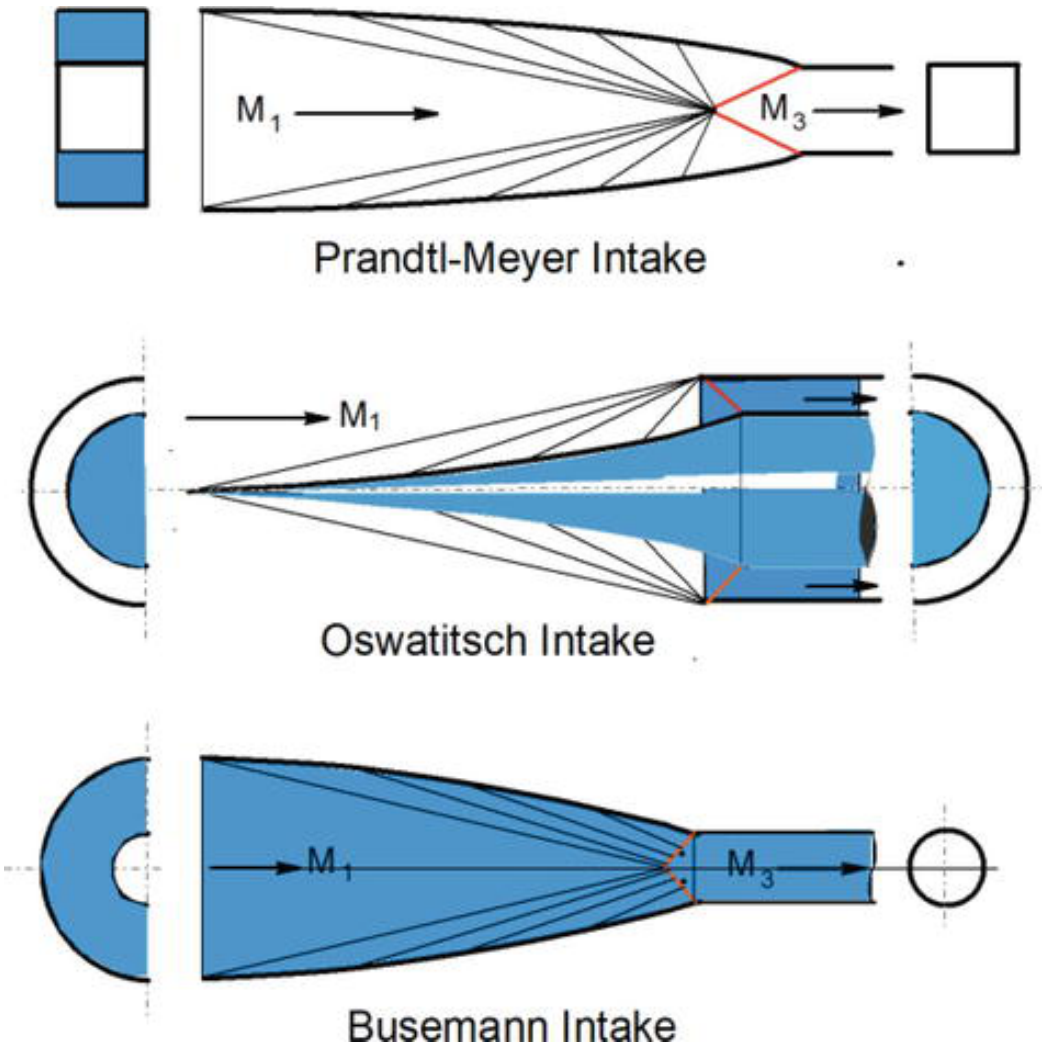

Figure 3-2: Rectangular, Oswatitsch, and Busemann inlet designs

For the purposes of this model, the objective is to estimate the pressure recovery of a certain design and its associated losses. There exists certain levels of modeling capability, ranging from very simple empirical models all the way to advanced Direct Navier-Stokes simulations. However, with increasing demand for detailed analysis, the input to the program will require more geometric input. Ultimately, there is no replacement for physical tests at flight conditions, however, some inlet models will be proposed and compared.

3.2 MIL- Spec E5007D Inlet Model

The MIL-Spec (short for Military Specification) inlet model is an empirically derived equation that gives a conservative estimate of a generic supersonic and hypersonic engine inlet. The purpose of this specification was so that engine designs from different manufacturers could be readily compared at various inlet conditions. As such, the MIL-E5007D specifies the following inlet recoveries for various Mach number ranges. For $0 < M_0 < 1$:

$$\frac{P_{t2}}{P_{t0}} = 1 \tag{3.1}$$

For $1 < M_0 < 5$:

$$\frac{P_{t2}}{P_{t0}} = 1 - .0776(M_0 - 1)^{1}.35 \tag{3.2}$$

For $M_0 > 5$:

$$\frac{P_{t2}}{P_{t0}} = \frac{800}{M_0^4 + 935} \tag{3.3}$$

For a range of $0 < M_0 < 10$, we can visualize this model graphically:

Here, we can readily see how the MIL-SPEC Inlet model predicts high stagnation pressure losses for a hypersonic vehicle. By $M_0 = 5$, nearly 50 percent of the flows stagnation pressure is lost, which does not bode well for hypersonic operation. It is worth mentioning that this inlet model is essentially a curve fit of data available in the mid-70's, as such it is reasonable to conclude that with modern knowledge about hypersonic inlets, as well as real scramjets operating at high Mach number, that there are more accurate models. In the next section, another such model will be analyzed.

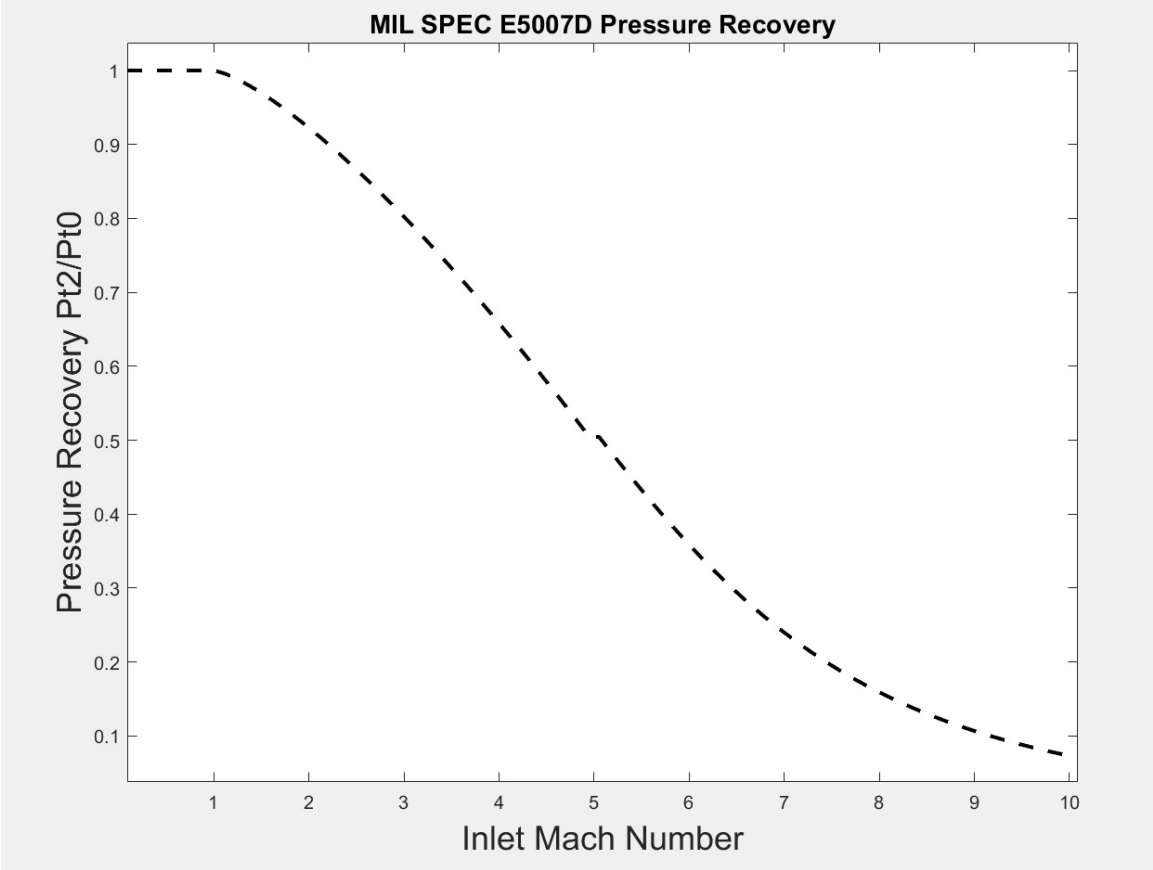

Figure 3-3: MIL SPEC Inlet Model

3.3 Kinetic Energy Efficiency Model

Here, a more advanced model of scramjet inlet pressure recovery is proposed. Its formulation is dependent on the definition of the "Kinetic Energy Efficiency" of a given inlet, defined as:

$$\eta_{KE} = \frac{h_{t0} - h(P_0, s_2)}{h_{t0} - h_0} \tag{3.4}$$

From Segal[9], it is explained as "a measure of kinetic energy loss that is due to the entropy increase during the compression process and includes both external and internal compression". Being that it is a definition based on thermodynamic quantities, the KE efficiency can be easily found for inlets of various designs and compared. As such, Van Wie[6] was able to compare multiple different inlet designs, both theoretical and physical, and compared their relative KE efficiencies:

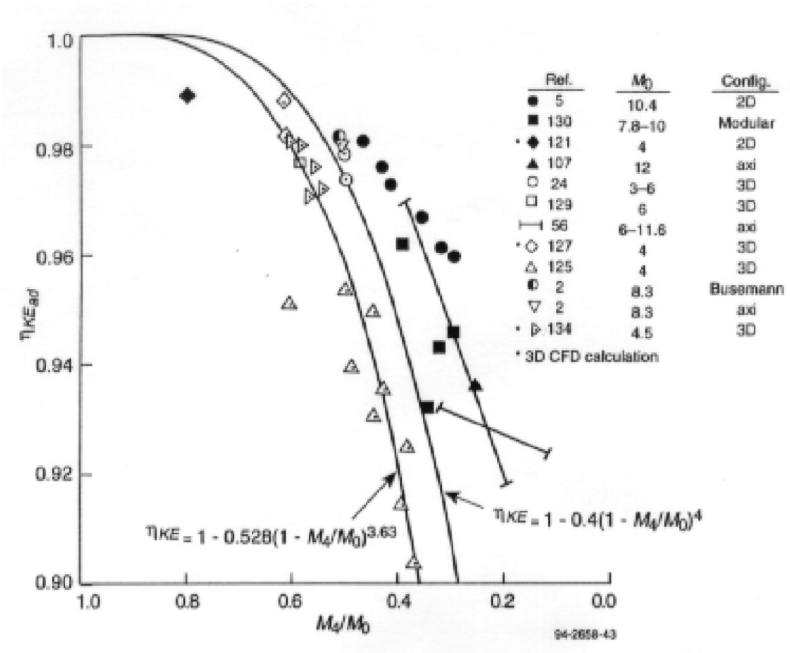

Figure 3-4: KE Efficiencies for different inlet designs [6]

What is important about these findings is that he established a correlation between inlets at different flight conditions, like Busemann inlets at hypersonic mach numbers, and found that the amount of compression demanded from the parameter M_2/M_0 (Station 4 in Van Wie is 2 in this Thesis) directly affects its KE efficiency. Moreover, this correlation is based on both experimental studies and computational data, lending credibility to their real world efficacy. Thus, we can interpret the results as those which exist for a well designed, theoretical inlet tuned for its flight condition. Based on the designer's choice for M_2/M_0, we can find η_{KE}:

$$\eta_{KE} = 1 - .4\left(1 - \frac{M_2}{M_0}\right)^4 \tag{3.5}$$

Assuming a calorically perfect gas, we are able to find the pressure recovery P_{t2}/P_{t0} through the following relation:

$$\eta_{KE} = 1 - \frac{2}{(\gamma - 1)M_0^2}\left[\left(\frac{Pt_0}{Pt_2}\right)^{\gamma - \frac{1}{\gamma}}\right] \tag{3.6}$$

Using a test value of $M_2 = 1.2$, and following some algebra, we can plot the

pressure recovery versus flight Mach number:

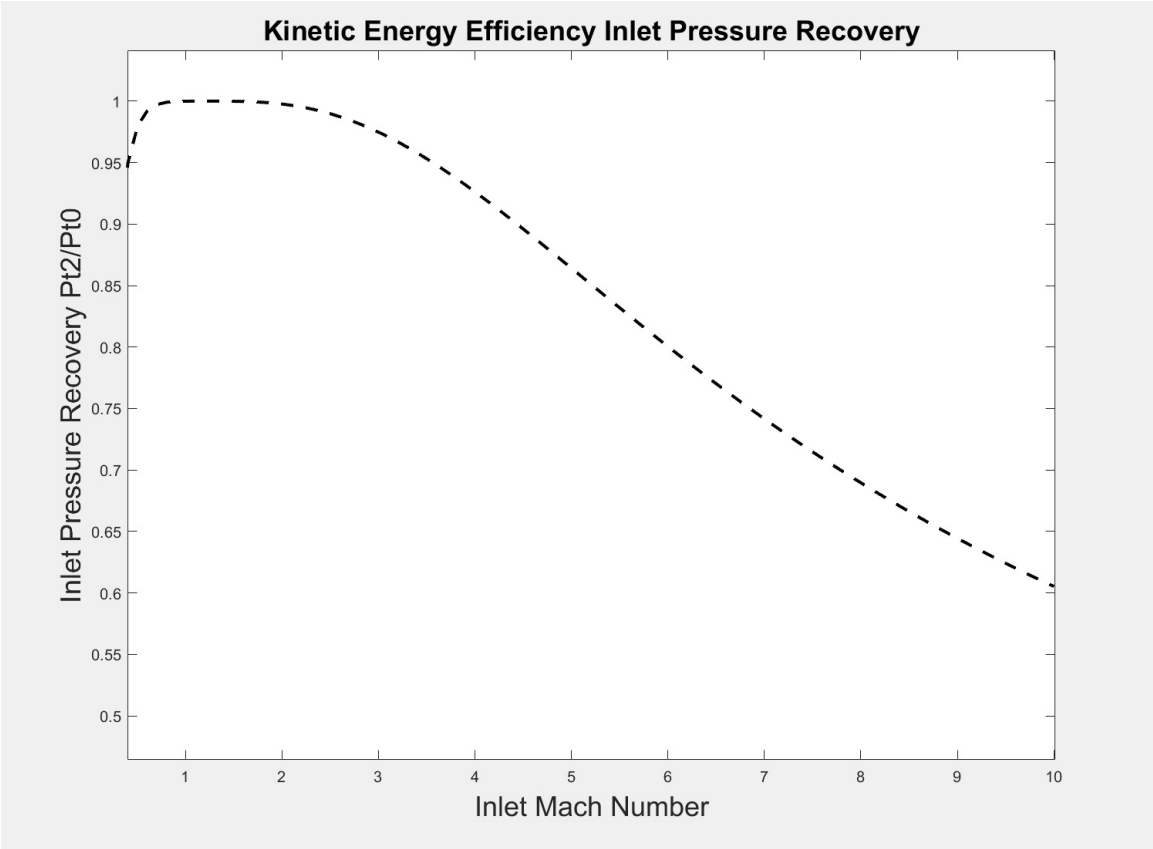

Figure 3-5: KE Efficiency Inlet Model

It is worth mentioning that this formulation does not account for any heat transfer which would be experienced by the through flow. More advanced formulations can account for this, however this model will assume the flow is adiabatic.

3.4 Inlet Model Comparison

To see how much these models differ in their prediction of pressure recovery, it is prudent to compare them side by side:

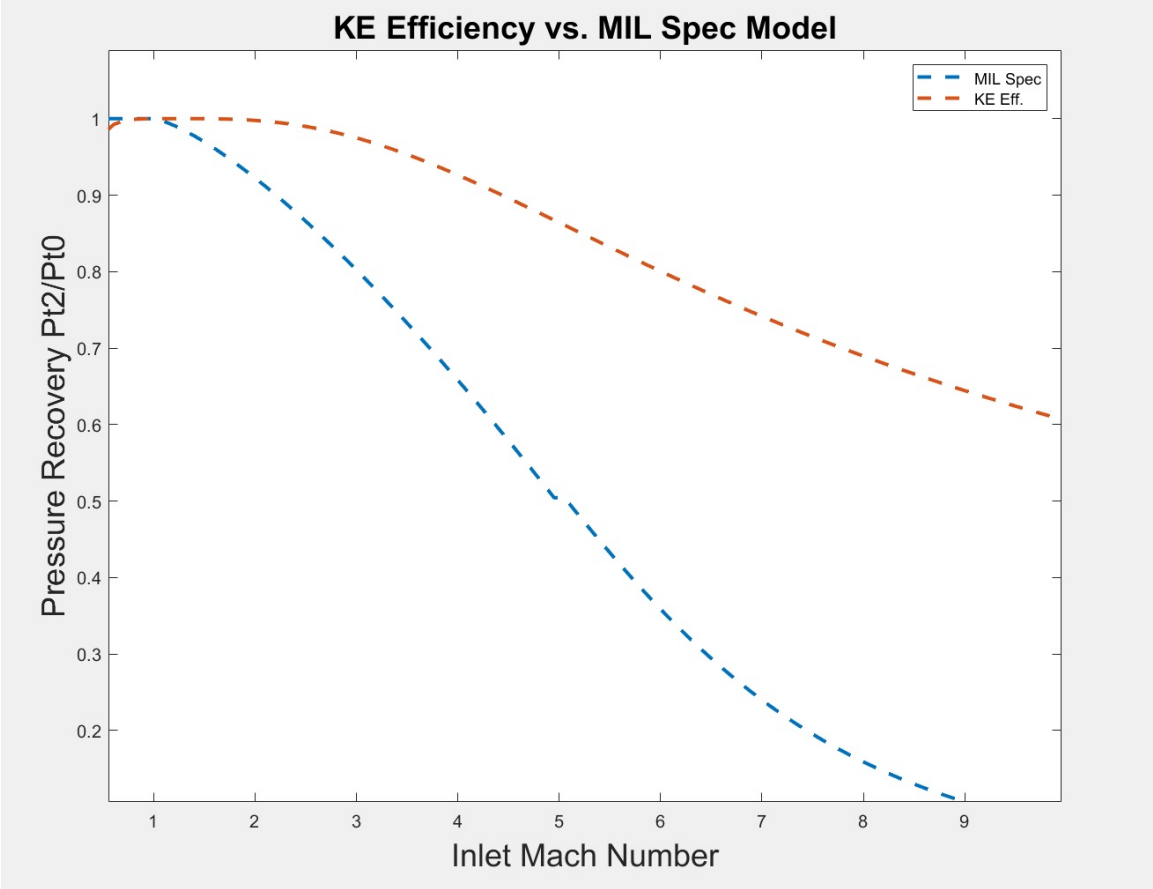

Figure 3-6: KE Efficiency vs. MIL Spec Inlet Model

Here we see how the MIL Spec model differs greatly by predicting much higher stagnation pressure drops in the supersonic and hypersonic flow regime. We also see that as a vehicle approaches hypersonic speeds, the maximum possible stagnation pressure recovery decreases linearly according to the KE efficiency model. Since the goal of the model is attempting to define the outer bounds of performance, the KE Efficiency model will be selected to perform the calculations.

Chapter 4

Isolator Model

4.1 1D Flow Equations

To set the stage for the subsequent analysis, the foundational 1D flow equations of the isolator and combustor model will be described first. These equations will then be modified for both the components as they pertain to each one's peculiarities. To begin, we first create an abstraction of a channel of varying area and of differential length dx. In this channel, a control volume is drawn and the various thermodynamic quantities of interest are noted: A, p, T, ρ, u, and M. From Internal Flow[7], a useful diagram is borrowed:

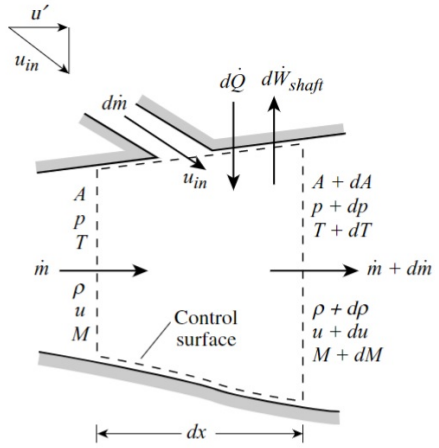

Figure 4-1: Control Volume [7]

For the sake of this analysis, the following assumptions shall be made:

1. The flow is inviscid
2. There is no mass addition
3. There is no heat transfer to the walls
4. There is no work exchange with the fluid
5. There are no body forces on the fluid
6. The flow is fully attached and steady
7. Gas constants R, c_p, and γ remain constant

Presented in differential form, we begin with a statement about the Conservation of Mass within the control volume:

$$\frac{d\rho}{\rho} + \frac{dU}{U} + \frac{dA}{A} = 0 \tag{4.1}$$

Next, we investigate the momentum of the fluid. Using the same control volume, the following force balance is established:

$$(\rho U dU + dp)A = -\tau_w dA_w \tag{4.2}$$

Wall shear stress is related to the skin friction Coefficient C_f by

$$\tau_w = C_f \rho \frac{U^2}{2} \tag{4.3}$$

and wetted area A_w by

$$A_w = 4A\frac{dx}{D} \tag{4.4}$$

where D is the hydraulic diameter of the channel. From a simple conversion of $\rho u^2 = \gamma p M^2$, and combining 4.2-4.4, we get:

$$\frac{dU}{U} + \frac{1}{\gamma M^2}\frac{dp}{p} + 2C_f\frac{dx}{D} = 0 \tag{4.5}$$

From Conservation of Energy and the definition of stagnation temperature, the next relation is defined for the control volume:

$$\frac{dT}{T} + \frac{\gamma - 1}{2}M^2\frac{dU^2}{U^2} = \left(1 + M^2\frac{\gamma - 1}{2}\right)\frac{dT_t}{T_t} \tag{4.6}$$

Equations (4.1), (4.5), and (4.6) describe the physics of the fluid in the control volume. In order to complete the equation set, we require an equation of state and a definition. This is given by the Ideal Gas Law in differential form:

$$\frac{dp}{p} = \frac{d\rho}{\rho} + \frac{dT}{T} \tag{4.7}$$

and the definition of Mach number:

$$\frac{dM^2}{M^2} + \frac{dT}{T} = \frac{dU^2}{U^2} \tag{4.8}$$

At last, we can combine all these equations to arrive at our differential 1-D flow equations that account for stagnation temperature change, friction, and area change:

$$\frac{dM^2}{M^2} = \frac{1 + \frac{\gamma-1}{2}M^2}{1 - M^2}\left[(1 + \gamma M^2)\frac{dT_t}{T_t} - 2\frac{dA}{A} + 4\gamma M^2 C_f\frac{dx}{D}\right] \tag{4.9}$$

$$\frac{dp_t}{p_t} = \left(-\frac{\gamma M^2}{2}\right)\left(\frac{dT_t}{T_t} + 4C_f\frac{dx}{D}\right) \tag{4.10}$$

One important aspect of these equations is that both dA/A and dT_t/T_t will be treated as independent inputs for the model - that is, the user will have the ability to modify these for the purposes of flow analysis and design. Another aspect is that these equations are truncated versions of Shapiro's influence coefficient matrix[15]. Relaxing assumptions 2 - 5 and performing the same analysis will arrive at those formulations.

4.1.1 Numerical Solutions for 1D Flow Equations

The solution scheme for these non-linear Ordinary Differential Equations will be similar for both the isolator and combustor calculations. First, we would like to racast these equations in terms of spatial gradients, as this model is one dimensional in the axial direction. Since $dM^2/M^2 = 2dM/dM$, we can rewrite (4.9) by differentiating with respect to dx:

$$\frac{dM}{dx} = M\frac{1+\frac{\gamma-1}{2}M^2}{1-M^2}\left[\frac{1+\gamma M^2}{2}\frac{dT_t}{T_t} - \frac{1}{A}\frac{dA}{dx} + \frac{2\gamma M^2 C_f}{D}\right] \tag{4.11}$$

For the numerical solution, by recognizing that this equation is a non-linear, first order ODE, the most obvious solution scheme is a 4th Order Runge-Kutta process. A 4th order scheme was chosen due to the stiffness of the ODE. For this equation

$$dM = f(x, M), y(x_0), M_0 \tag{4.12}$$

We then predict each successive value as we move along in x using the following scheme:

$$M_{n+1} = M_n + \frac{1}{6}h\Big(k_1 + 2k_2 + 2k_3 + k_4\Big) \tag{4.13}$$

where

$$x_{n+1} = x_n + h \tag{4.14}$$

$$k_1 = f(x_n, M_n) \tag{4.15}$$

$$k_2 = f\Big(x_n + \frac{h}{2}, M_n + \frac{hk_1}{2}\Big) \tag{4.16}$$

$$k_3 = f\Big(x_n + \frac{h}{2}, M_n + \frac{hk_2}{2}\Big) \tag{4.17}$$

$$k_4 = f(x_n + h, M_n + hk_3) \tag{4.18}$$

With the numerical scheme defined, a few "test" values are required in order to fully define the problem. The purpose of this exercise is to establish that the numerical scheme is stable and reports the correct trends for the given fluid input. If we can establish that the code works correctly, we are able to proceed with adding complexity to the system.

The values which need definition are friction coefficient C_f, isolator inlet Mach number M_2, isolator inlet pressure p, ratio of specific heats γ, hydraulic diameter D, flow through area A, and overall isolator/combustor length, defined by $x_4 - x_2$, and where x_3 is the threshold between the two. For ease of calculation, $x_2 = 0$. Additionally, the code requires input for dA/dx and dT_t/dx. These shall be user defined functions, and will be a topic of great importance later in the chapter. For now, they will be arbitrarily defined for the sake of diagnostics. To begin, a very simple case is defined: For a supersonic inlet Mach number, friction and heat addition will be turned off, and the area remains constant.

Table 4.1: Test Values

Variable	M_2	C_f	γ	A_0	x_3	x_4	dA/dx	dTt/dx
Value	2.0	0.0	1.4	.0028	.2	.5	0	0

The results of this test run are now plotted. Quantities are non-dimensionalized for ease of comparison.

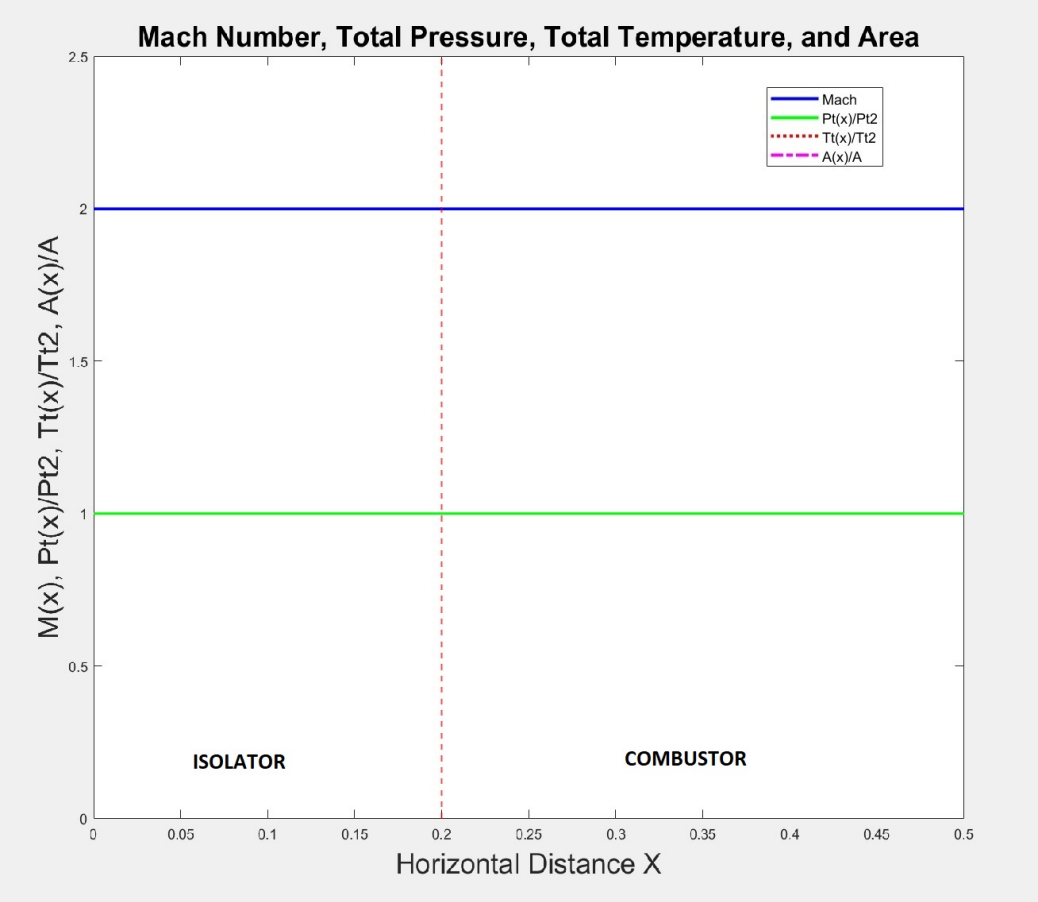

Figure 4-2: Test Run

As expected, with no heat addition, friction, or area change, we expect the Mach number to remain constant and total pressure to remain unchanged. Thus we are able to confirm that the program does not give false values for undisturbed flow. Next, we will investigate supersonic flow with friction, best known as Fanno flow. The input values are:

Table 4.2: Fanno flow input

Variable	M_2	C_f	γ	A_0	x_3	x_4	dA/dx	dTt/dx
Value	2.0	0.002	1.4	.0028	.2	.5	0	0

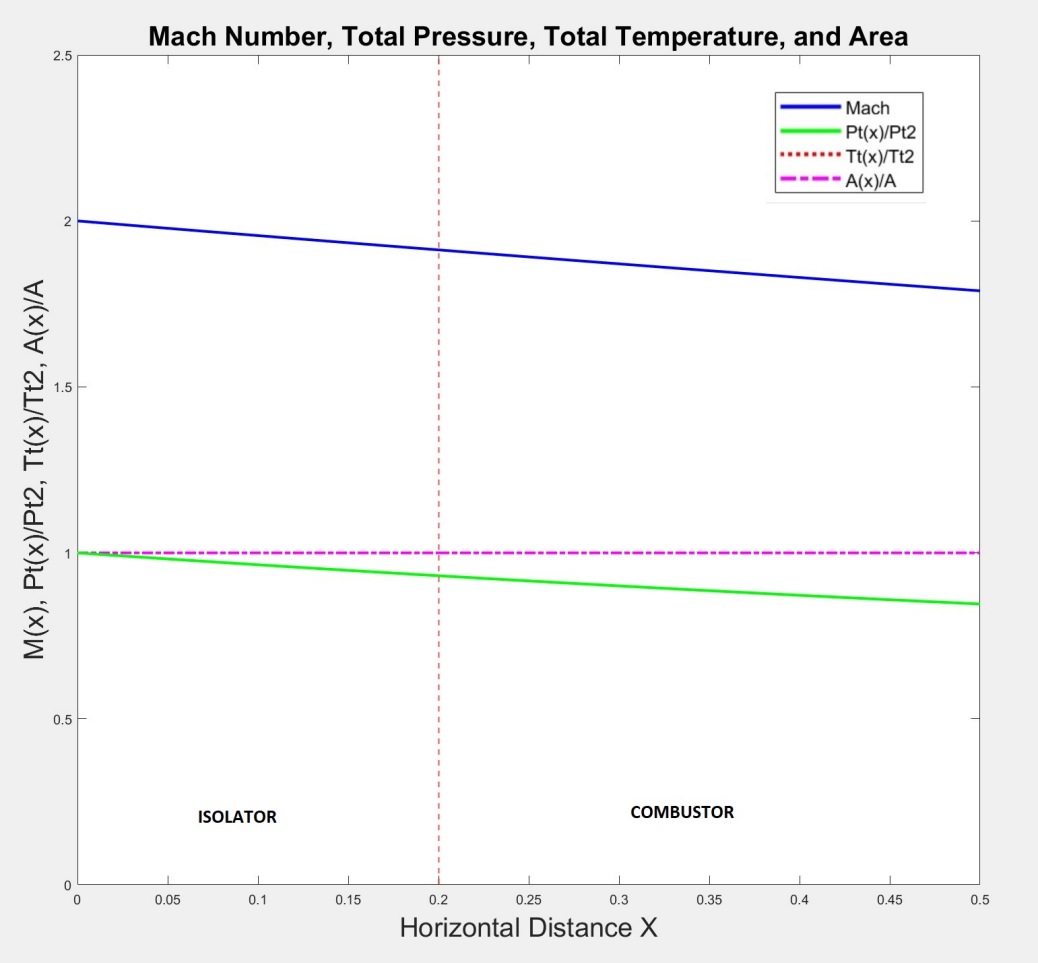

Figure 4-3: Fanno flow

Here, we observe that due to the influence of friction, the Mach number decreases as well as the stagnation pressure, indicating a loss in fluid momentum. The trend observed is exactly as expected. Next, Rayleigh flow shall be investigated, which indicates heat release in the combustor in the absence of friction and area change. The input is as follows:

Table 4.3: Rayleigh flow input

Variable	M_2	C_f	γ	A_0	x_3	x_4	dA/dx	dTt/dx
Value	2.0	0.002	1.4	.0028	.2	.5	0	Linear

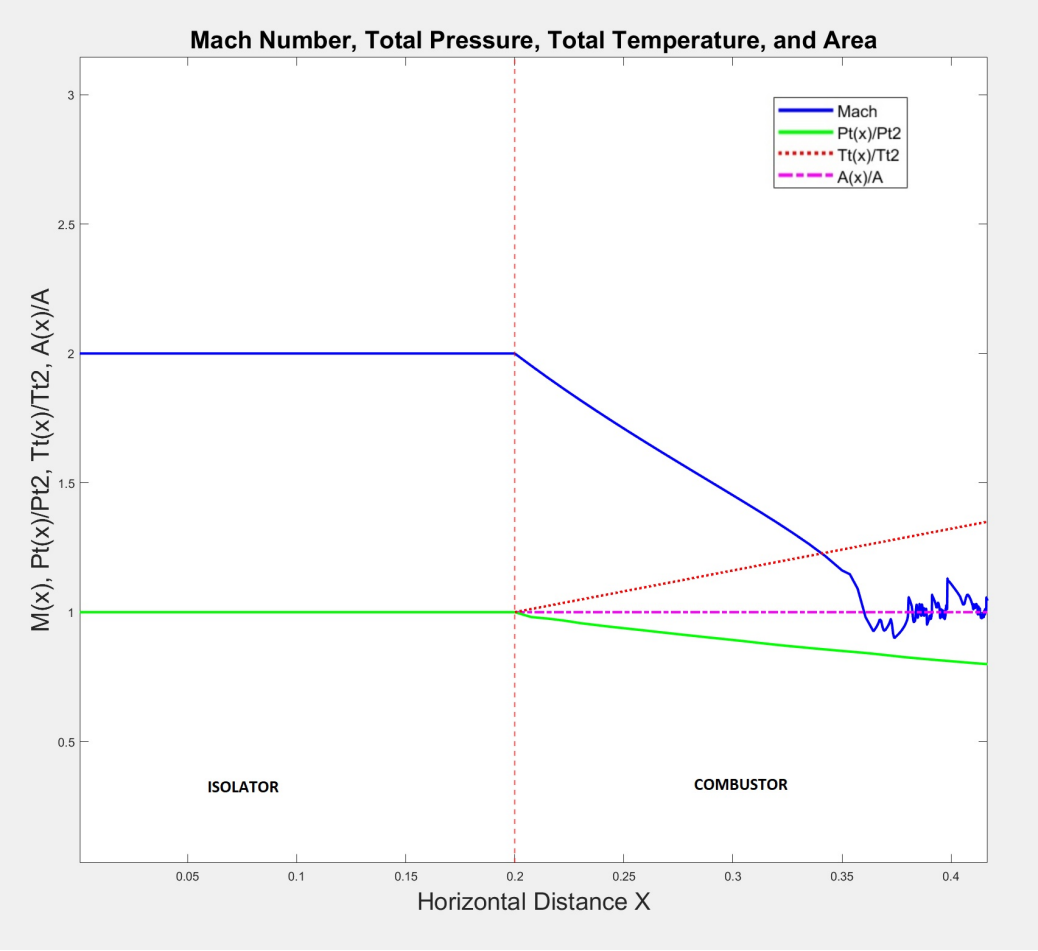

Figure 4-4: Rayleigh flow

Here, we readily see the trend expected from Rayleigh flow: Lack of friction causes no change in the isolator, but heat release causes rapid drop of Mach number in the combustor as well as an accompanying drop in stagnation pressure. In this case, a linear heat release in the combustor was imposed, and interestingly, the drop in Mach number and stagnation temperature appear linear as well. Towards the end of the combustor "noise" is observed for the Mach number, and it can be concluded that this is due to "thermal choke". In other words, the Mach number has been reduced to unity, and will remain there even as heat is continually added. In order to prevent this phenomenon, designers schedule the combustor area to increase so that the flow can expand while heat is released. As a result, the flow will remain supersonic and unchoked, thus minimizing losses. In order to model this phenomenon, a linear area

schedule shall be implemented along with a linear temperature schedule and constant friction. The input is given as:

Table 4.4: Complete flow input

Variable	M_2	C_f	γ	A_0	x_3	x_4	dA/dx	dTt/dx
Value	2.0	0.002	1.4	.0028	.2	.5	2:1	Linear

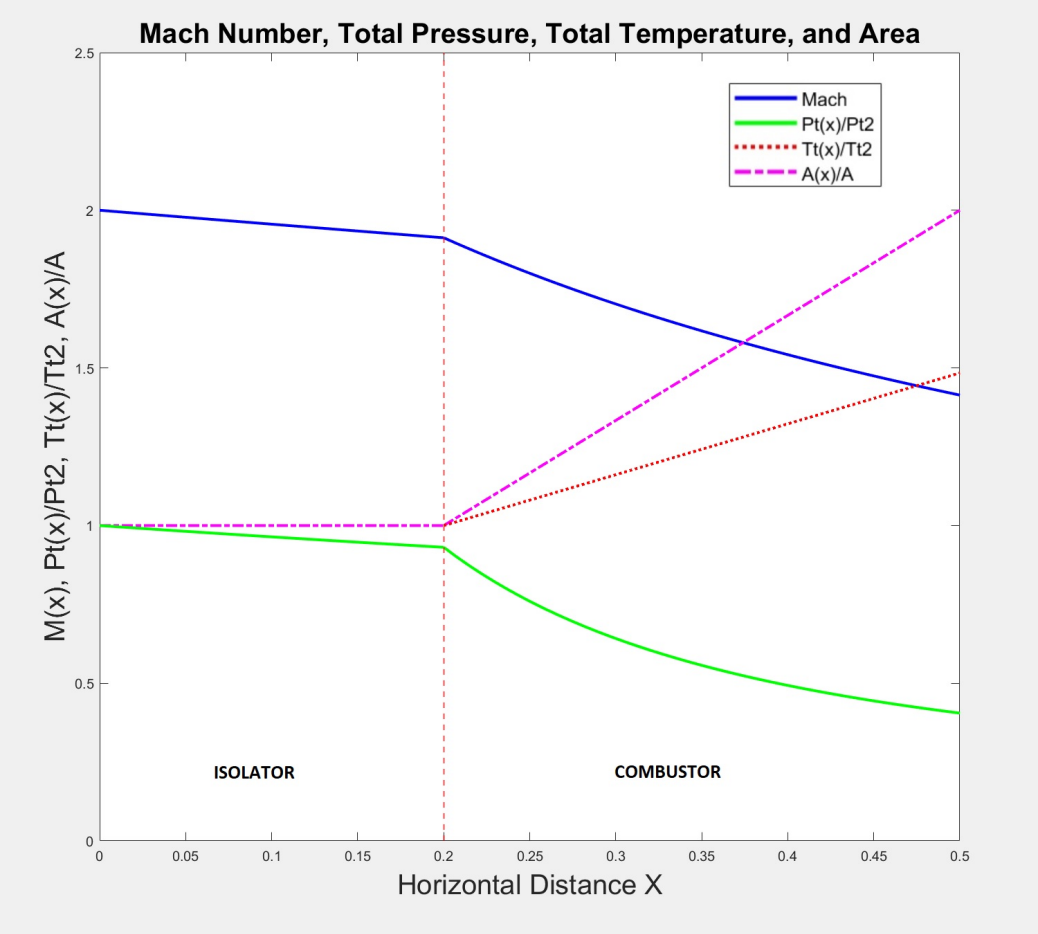

Figure 4-5: Complete flow description

As expected, doubling the area across the combustor prevents the flow from choking, and prepares it for further expansion in the nozzle downstream. The plot accurately captures the trends of the complicated physics associated with supersonic flow. We also observe that stagnation pressure losses approach 50 percent; this is unfortunately the inevitable result of heat release in a supersonic flow. Since we know that

$dp_t \sim M^2$, a scramjet designer will want the combustor entrance Mach number to be as low as possible while remaining unchoked for steady operation. Thus, it is very important that the area schedule dA/dx account for the heat release dT_t/dx. All these competing effects and the designer's ability to predict them accurately remain the primary challenge in scramjet design. The specific aspects of these design challenges facing the isolator and combustor will now be explored in the subsequent sections.

4.2 Isolator Model

For many scramjet designs, the system requires that the engine have the capability to operate in a variety of flight Mach numbers, oftentimes ranging from $M_0 = 4$ to $M_0 = 10$. When operating in such a range, the scramjet's combustor must be able to accommodate a wide variety of Mach numbers into itself, requiring that it be able to perform its goal without upsetting the upstream flow. When heat is released by combustion in a supersonic flow, a large pressure gradient is established, sometimes great enough to cause flow separation to the incoming fluid. If this pressure gradient is large enough to cause this separation, a series of shockwaves are produced upstream of the combustor, which in turn further compress the incoming fluid. Left unchecked, these newly created shockwaves can travel into the inlet and potentially disrupt the carefully balanced oblique shock waves found in the inlet. Thus, in order to contain this phenomenon, a device called an "isolator" is implemented along with the combustor. The idea is that if a flow separation and ensuing shock train occur, it is relegated to the confines of the isolator, thus allowing the combustor and inlet to operate as normal, as if they were "isolated" from one another.

From fig. 4-6, we have a visualization of the the separated flow within the isolator, and we can observe several phenomena: A series of shock waves exist, which interact with the thick boundary layers formed near the wall - a key representation of shock-boundary layer interaction. Additionally, the effective flow through area of the inviscid flow has been reduced significantly, such that it will have a strong effect on the Mach number and potentially mass flow rate. In essence, the shock train behavior of a

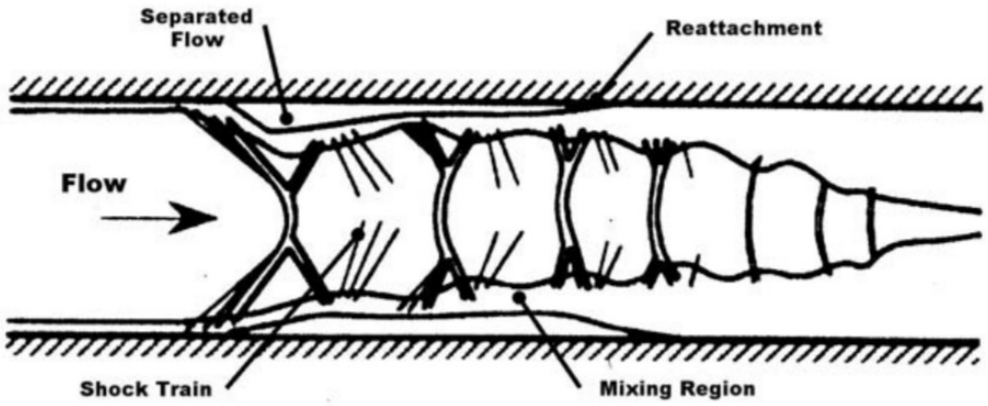

Figure 4-6: Shock Train in an isolator [3]

separated flow in an isolator is as if the scramjet had variable geometry - a fascinating and crucial aspect of their operation. Thus, it would be beneficial for this model to capture and analyze this effect to aid in its analysis. Much of the subsequent work borrows heavily from Waltrup and Billig[8], and Smart[3], who will be referenced frequently in this section.

In the 1970's, Waltrup and Billig performed many experiments with isolators containing the distinctive separated flow. They were able to find a correlation between an imposed pressure rise dP/P, the distance s over which the resulting shock train spread, and the geometric features of the duct. The equation they found was:

$$50\left[\frac{\Delta P}{P}\right] + 170\left[\frac{\Delta P}{P}\right]^2 = \frac{s(M^2-1)(Re_\theta)^{1/4}}{D^{1/2}\theta^{1/2}} \tag{4.19}$$

Plotted against multiple test cases, the quadratic relation correlated very well with the data taken from the shock train.

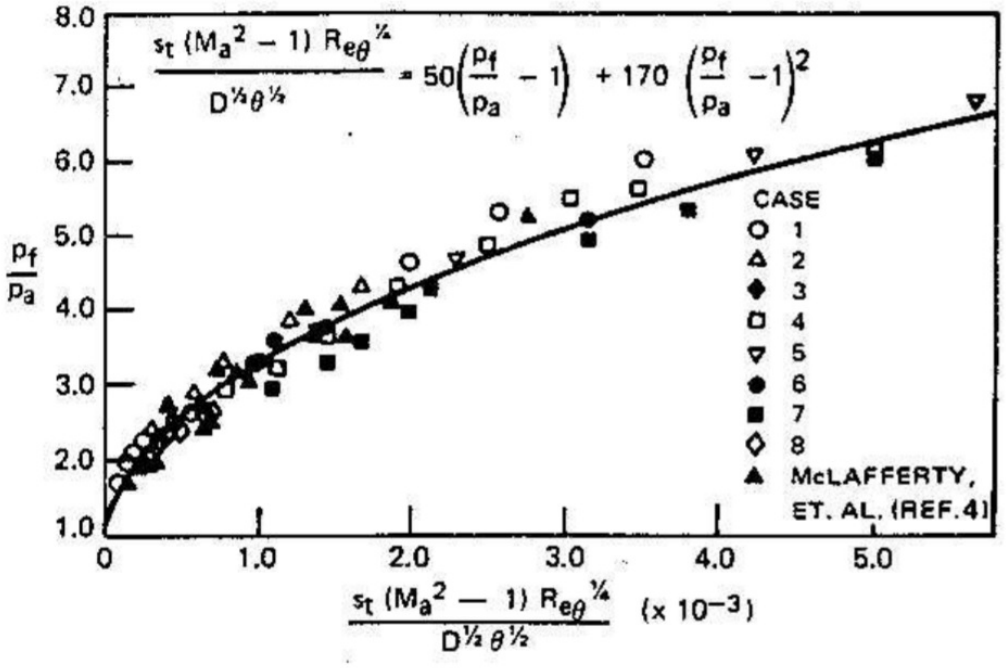

Figure 4-7: Shock Train Correlation [8]

Form this correlation, it was found that for a given pressure rise $\Delta P/P$, (assuming it was large enough to cause flow separation), the distance over which the shock train spread s was directly proportional to the momentum thickness θ and the duct diameter D, and inversely proportional to the Mach number and Reynolds number. From [3], an explanation of this correlation is offered: "It has been postulated by many authors that the pressure gradient experience by the core flow in the duct must be equal to the pressure gradient that can be supported by shear in the separated region." From this leap of faith, a differential relation can be derived for the pressure rise in the duct [3]:

$$\frac{dP}{dx} \sim \frac{89 C_f}{D}\left(\frac{\rho U^2}{2}\right) \tag{4.20}$$

With these relations established, it is now possible to modify our original 1D Flow equations to model separated flow in a duct.

4.2.1 Modified 1D Flow Equations

In order to establish the analytical flow equations which describe separated flow, the setup is much the same as from section 4.1.1: Conservation of Mass, Momentum, and Energy in combination with an equation of state and definition of speed of sound provide the fundamental groundwork for the analysis. However, we now have a new pressure term to deal with as well as an effective flow through area which is different to the geometric area. Borrowing a diagram from Smart, the following graphic describes the new control volume setup:

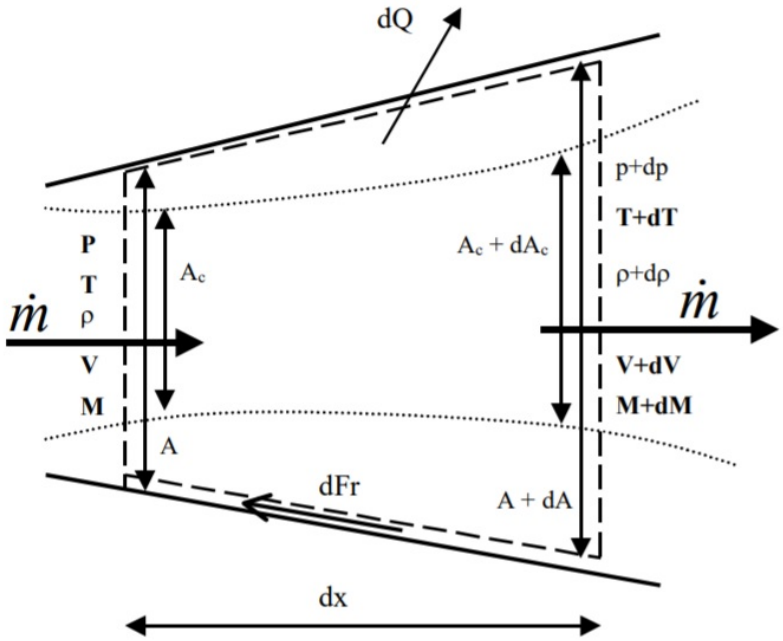

Figure 4-8: Control volume with separated flow [3]

From this figure, a new variable A_c is established, which represents the true flow through area due to blockage. As such, the non-dimensional parameter A_c/A will become a key feature of this analysis. Performing the same mathematics as before with the attached flow equations, and combining them with Eq. (4.20), we now arrive at our modified 1D flow equation for Mach number:

$$\frac{dM^2}{M^2} = -\left(1 + \frac{\gamma - 1}{2}M^2\right)\left[\frac{dT_t}{T_t} + \frac{dp/p}{\frac{\gamma M^2 A_c}{2A}} + \frac{4\gamma M^2 C_f \frac{dx}{D}}{\frac{A_c}{A}}\right] \tag{4.21}$$

In addition to the equation for Mach number, we also require a relation for $d(A_c/A)/(A_c/A)$. After a lot of algebra, this relation is found:

$$\frac{d(A_c/A)}{A_c/A} = \left[\frac{1 - M^2\{1 - \gamma(1 - A_c/A)\}}{\gamma M^2 A_c/A}\right]\frac{dp}{p} + \left(\frac{1 + (\gamma - 1)M^2}{2A_c/A}\right)4C_f\frac{dx}{D} + \left(1 + \frac{\gamma - 1}{2}M^2\right)\frac{dT_t}{T_t} \tag{4.22}$$

Just like before, user input functions for area scheduling and temperature distribution are required to complete the equation set. An important note about these equations is that they deal directly with the inviscid flow and how it interacts with the separated regions in the duct, it is not calculating the specifics of the separated boundary layer itself.

4.2.2 Numerical Solution to Modified 1D Flow Equations

In a similar way as before, the best numerical solver for these nonlinear ODEs is a 4th order Runge-Kutta scheme. However, the modified flow equations pose an extra level of complexity: they are coupled ODE's. First, recasting these equations in terms of a spatial derivative is necessary. Since this will model flow in the isolator, the term for heat addition will be removed.

$$\frac{dP}{P} \sim \frac{89 C_f \gamma M^2 dx}{2}\sqrt{\frac{\pi}{4A}} \tag{4.22}$$

$$\frac{dM^2}{dx} = -M^2\left(1 + \frac{\gamma - 1}{2}M^2\right)\left[\frac{93 C_f \sqrt{\frac{\pi}{4A}}}{\frac{A_c}{A}}\right] \tag{4.23}$$

$$\frac{d(A_c/A)}{dx} = \frac{89 C_f \gamma M^2}{2}\sqrt{\frac{\pi}{4A}}\left[\frac{1 - M^2(1 - \gamma(1 - A_c/A))}{\gamma M^2}\right] + 4C_f\sqrt{\frac{\pi}{4A}}\left[\frac{1 + (\gamma - 1)M^2}{2}\right] \tag{4.24}$$

Now, the problem becomes:

$$dM^2 = f(x, M^2, A_c/A), y(x_0), M_0^2, A_c/A \tag{4.25}$$

$$d(A_c/A) = f(x, M^2, A_c/A), y(x_0), M_0^2, A_c/A \tag{4.26}$$

Using MATLAB's built in ODE45 solver, these two coupled ODE's can be readily solved. In order to test the isolator model with separated flow, a simple test case with zero friction is applied:

Table 4.5: Test Values

Variable	M_2	C_f	γ	A_0	x_2	x_3	dA/dx	dTt/dx
Value	2.0	0.0	1.4	.0028	0	.2	0	0

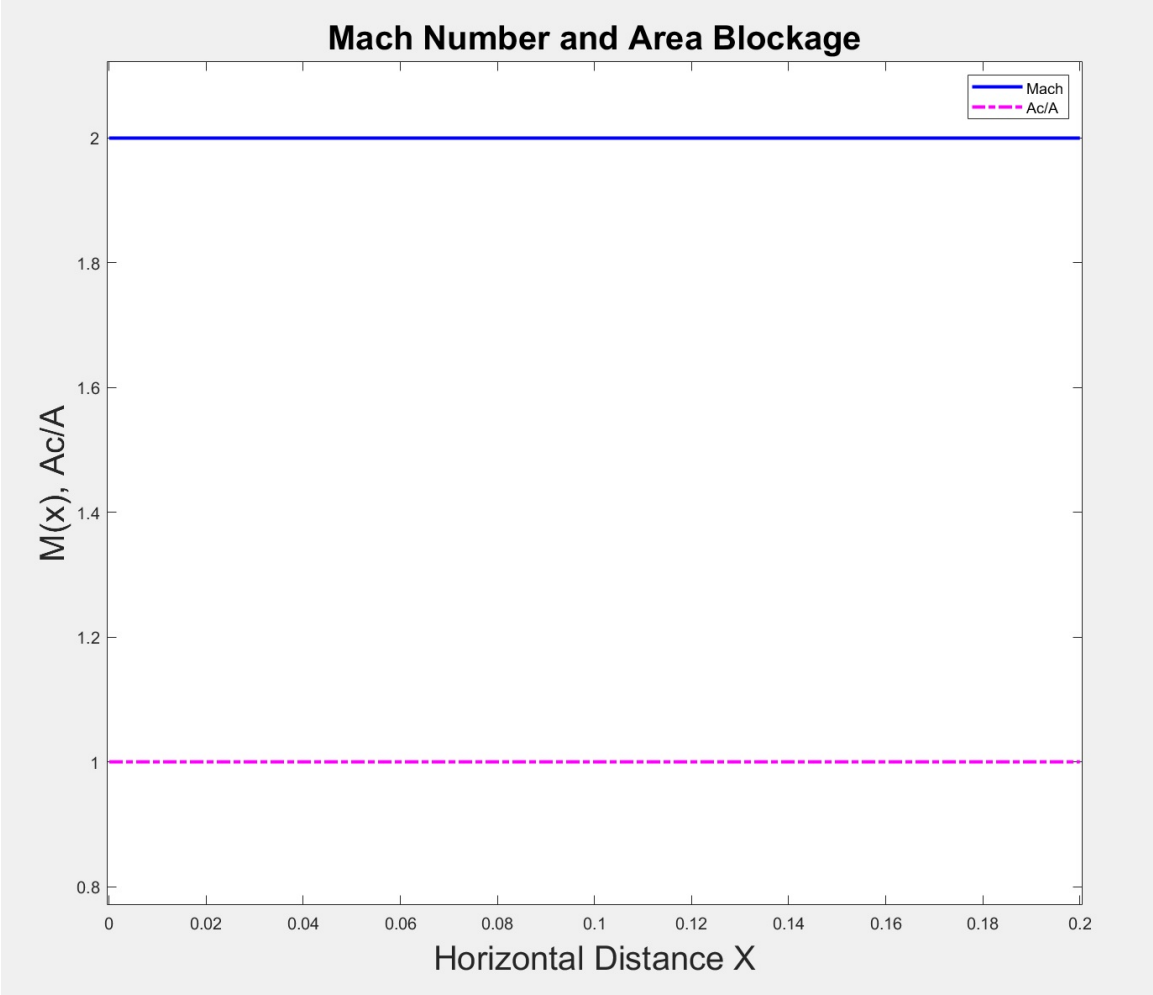

Figure 4-9: Test case with zero friction

As expected, with zero friction the flow remains perfectly attached in the isolator, and both the Mach number and A_c/A remain constant along its span. Next, we will enable friction and observe how these equations model "blocked" flow in a duct with separation:

Table 4.6: Separated flow with friction values

Variable	M_2	C_f	γ	A_0	x_2	x_3	dA/dx	dTt/dx
Value	2.0	0.002	1.4	.0028	0	.2	0	0

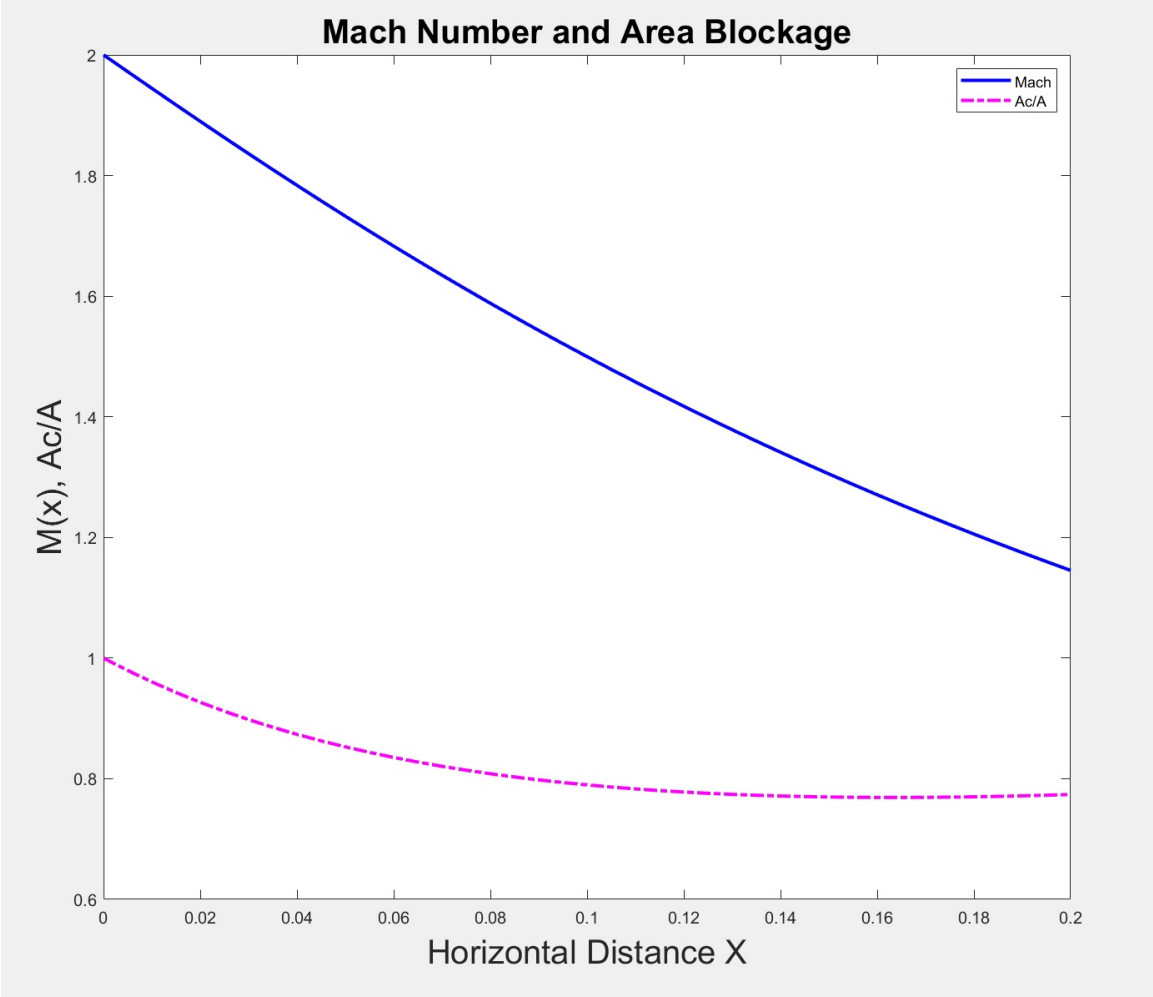

Figure 4-10: Isolator blockage

Here, we observe a concurrent drop in Mach number and A_c/A, indicating both losses in fluid momentum and boundary layer growth in the duct. It appears that towards the end of the isolator, nearly 20 percent of the flow through area is blocked, but this blockage reaches a steady state towards the end. As postulated from before, the imposed pressure gradient due to the pressure rise in the combustor is balanced out by the pressure gradient supported by the shear layer in the duct. Thus, we now have a more complete physical description of flow in the isolator by modeling separated flow. This capability now permits analysis to fine tune the length of the isolator [16].

Chapter 5

Combustion Model

5.1 Elements of Supersonic Combustion

At the heart of the scramjet lies the combustor, where flow traveling at supersonic speeds must be able to successfully mix with fuel, hold a steady flame, and release heat with as high efficiency as possible. Due to the large range of hypersonic flow in which scramjets must operate, the thermodynamic conditions of the combustor can change quite significantly, thus a combustor suited for one range of flight Mach numbers may not be well suited for another. At lower flight Mach numbers, heat release compared to flow enthalpy in the combustor can be large, and as demonstrated on Chapter 4, the resulting pressure rise can cause flow separation in the isolator. In the regime of extremely high flight Mach number, some as high as Mach 20+, relative flow enthalpy greatly exceeds heat deposition, such that the combustor design is less concerned with sharp pressure rises but rather management of hypersonic flows and accomplishing successful maintenance of the flame. The aerothermodynamic processes found in the combustor are complex and closely related[], so in order to model the combustion chamber of the scramjet, some explanations of the involved physics are presented.

5.1.1 Time Scales

With average Mach numbers in a scramjet anywhere in the supersonic region, the time scales associated with the flow become essential for initial combustor analysis. Given that most scramjet engine designs are on the order of 1.0 m[1], the associated flow through times are on the order of $\sim$ $1ms$[9] Thus, the reaction times of the combustion process must be addressed to evaluate the efficacy of a given design and fueling scheme. Within this span of a few ms, fuel must mix with air as well as complete its reaction so that it can be successfully expanded through the nozzle. A figure explaining some of these time scales is offered by Warnatz et al.:

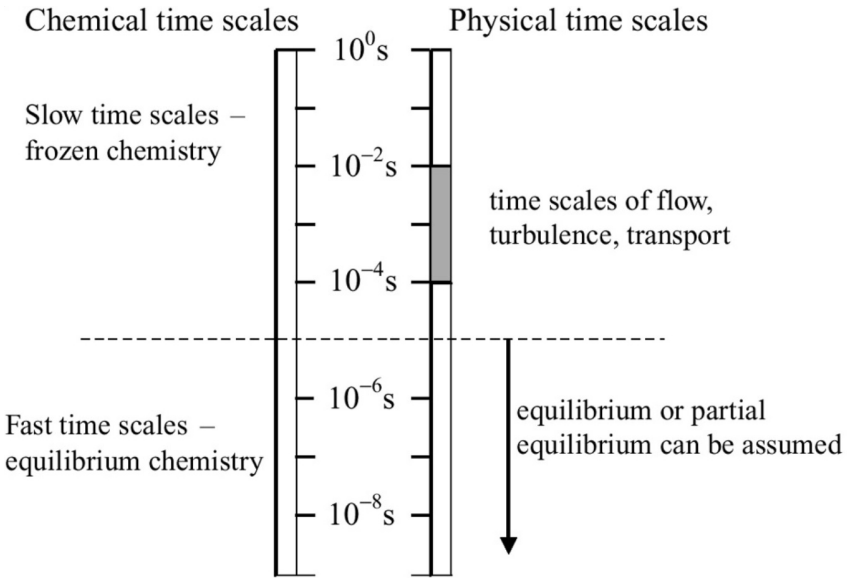

Figure 5-1: Flow time scales [9]

A common way to represent these time scales is with the Damköhler number (Da), which is typically a ratio of Da = Reaction rate/Convective mass transport rate. In terms of time scales, the Damköhler number can also be written as

$$Da = \frac{\tau_{flow}}{\tau_{rxn}} \tag{5.1}$$

Its importance is that it gives an intuitive idea about which physical process is dominant, whether its flow convection or chemical reaction. Thus, having a value for Da can help predict the chemical distribution in a given combustor flow. For $Da >>$

1, we can expect complete combustion and equilibrium conditions at combustor exit, and for $Da << 1$, reaction times are relatively slower than flow through times, so combustion products will still be reacting as the flow exits the engine. It turns out that for most conditions under which supersonic combustion occurs in a scramjet, the Damköhler numbers are of order unity ($Da \sim 1$)[]. From this insight, we know that both effects of convection and chemical reaction rate are important in combustor flow. Investigation into the timescales of the reaction can be found with chemical kinetic analysis, which will be expounded upon later in the chapter.

5.1.2 Fuel/Air Mixing

One of the biggest challenges facing scramjet design is the problem of fuel/air injection and mixing. Not only must fuel and air mix at the molecular level before ignition, it must do so within a relatively short distance and with minimal mixing losses from the turbulent wakes often used to achieve it. According to Segal, a common method to achieve this mixing is by injecting the fuel upstream of the combustor and perpendicular to the flow [9]. This causes "barrel shocks" to form which results in misaligned pressure and density gradients. This, in turn, creates vorticity in the flow which aids in achieving molecular mixing at the cost of fluid momentum.

$$\frac{d\omega}{dt} = \nabla p \times \nabla\left(\frac{1}{\rho}\right) \tag{5.2}$$

A good visual representation of this phenomenon is offered by Segal:

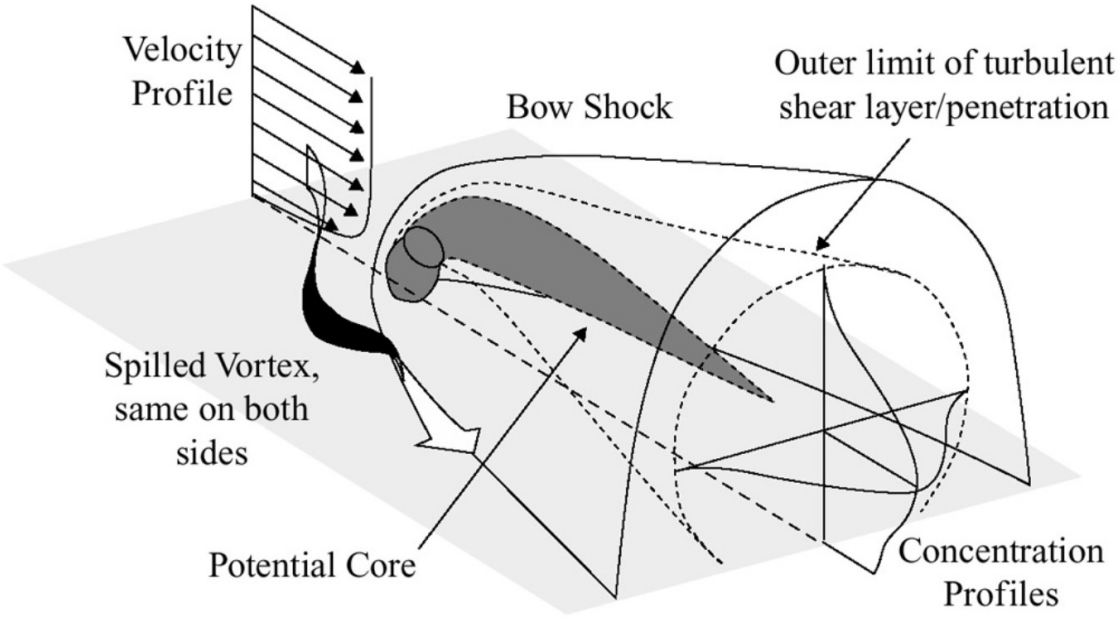

Figure 5-2: Fuel air mixing with transverse injection[9]

The complexity of fuel air mixing makes it a topic ripe for further research, however for the purposes of this model, it will be assumed that the mixture entering the combustor is already well mixed. It is however very important that careful consideration of the mixing dynamics is done during the design process so the scramjet is able to operate as it is envisioned.

5.2 Chemical Modeling

5.2.1 Overview

In order to model the chemical reactions taking place within a scramjet, several levels of complexity are described [17].

1. Perfect Gas Model: The most simple type of gas model comes from the assumption of a perfect gas. In this situation, the ratio of specific heats γ is assumed constant, as well as the composition of the gas itself. The assumption of a perfect gas greatly simplifies calculation complexity, and models certain processes

in turbomachinery quite well (such as flow through a compressor), however, the assumption of a perfect gas rapidly breaks down during a combustion process since gas composition is changing.

2. Frozen Gas Model: For this type of modeling, the gas composition is still assumed constant, but the assumption of constant γ is relaxed. This gives greater fidelity for calculations where flows are non reactive, such as nozzle flow, however falls short for in depth combustion analysis.

3. Equilibrium Gas Model: In this flow situation, it is assumed that along each axial position in the flow, the gas composition is in chemical equilibrium. By extension, thermodynamic quantities such as pressure and temperature can be used to find the composition of the flow.

4. Finite Rate Chemistry: A very in depth type of combustion analysis involves using finite rate chemistry to model gas composition as fuel and air react. In this situation, a chemical mechanism is proposed which describes how a a given fuel and oxidizer react with each other. The overall reaction is modeled as a series of intermediate reactions, whose rate of reaction depends on the relative concentrations, temperature, and pressure of the species. The difficulty in finite rate chemistry stems from the fact that the intermediate reactions are a series of coupled Ordinary Differential Equations whose time scales can be very orders of magnitude different than one another. Additionally, the mechanism itself may not be well suited for all situations, so care must be taken in deciding which mechanism to employ.

5.2.2 Fuel Choice

In order to evaluate the chemistry occurring in the combustor, a fuel choice is required. For many academic studies, hydrogen fuel (H_2) is picked due to its high adiabatic flame temperature, thus theoretically offering the highest Isp as a fuel choice. However, in practical implementation, hydrogen has significant drawbacks, such as the

fact that it must be stored cryogenically in liquid form, as well as the fact that it is relatively less dense than hydrocarbon based fuels, thus requiring larger storage tanks for the same amount of energy. As a result, researchers have considered studying the use of hydrocarbon based fuels in scramjet combustors due to size constraints. Some hydrocarbon fuels currently being investigated include Methane (CH_4) and Ethylene (C_2H_4), as well as kerosene. While hydrocarbon fuels have advantages compared to hydrogen, especially with respect to energy density, one drawback is that they have relatively lower ignition times [10].

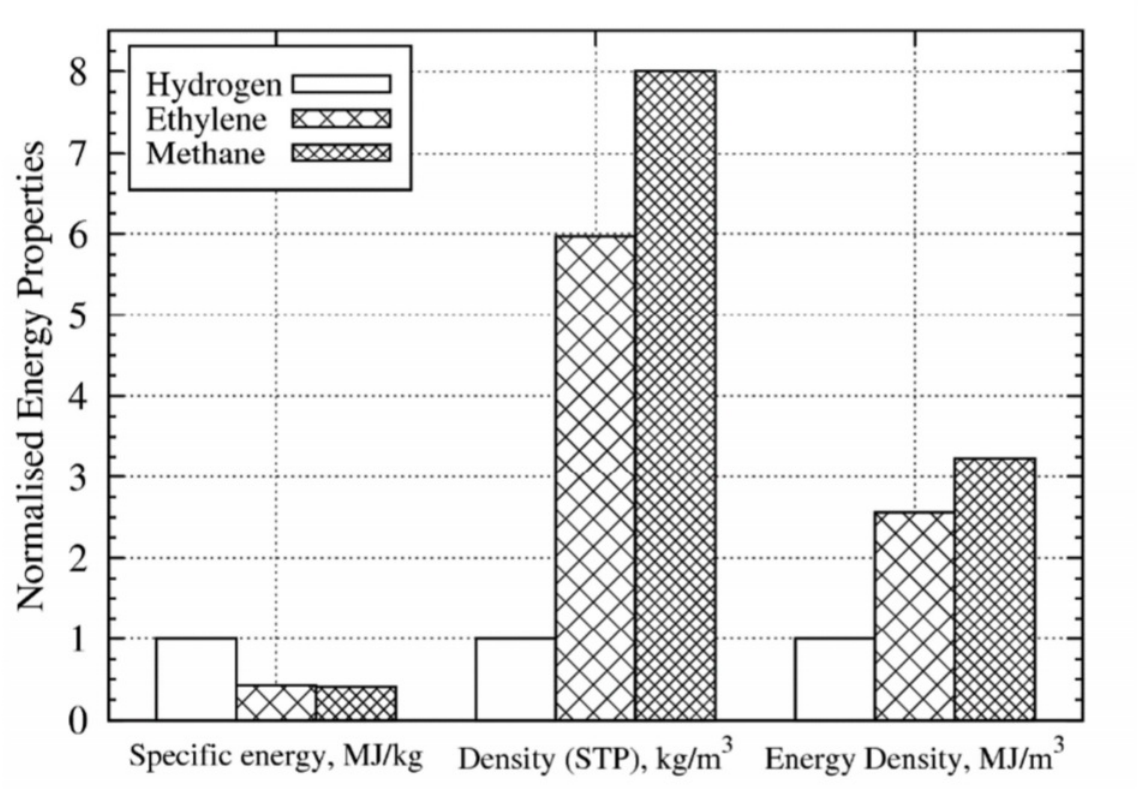

Figure 5-3: Normalized fuel energy and density comparisons[10]

For the purposes of this model, the chosen fuel for analysis will be ethylene. The reason stems from the fact that most 1D models have already analyzed hydrogen fuel, as well as the fact that ethylene is a thermal constituent for larger hydrocarbon fuels, such as JP4. What this combustion model seeks to find about ethylene combustion is what order of magnitude the ignition times occur, as well as an estimation of the heat

release profile necessary for the 1D model. By using empirical data from experiments done with ethylene as well as some elementary kinetic analysis, the 1D model can remain as informed as possible.

5.2.3 Chemical Kinetics of Ethylene

The purpose of analyzing the kinetics of ethylene is to first establish an idea for time scales. It is purported that ethylene is highly "reactive", that is, its ignition delay times are short thus making it well suited for high speed propulsion. Chemical kinetics can inform the ignition time τ_i, which can then be used in conjunction with the flow through time of the combustor to estimate the order of magnitude of its length scale[11]. In order to proceed with the analysis, a chemical mechanism of how ethylene reacts with air is necessary. The mechanisms which exist are very large, such as the one developed at UCSD which has 57 species and 268 reactions. For the sake of explanation, a simplified mechanism is demonstrated:

$$
\begin{aligned}
\mathrm{H} + \mathrm{O_2} &\rightarrow p\mathrm{OH} + p\mathrm{O} + (1-p)\,\mathrm{HO_2},\\
\mathrm{H_2O_2} &\rightarrow 2\mathrm{OH},\\
\mathrm{C_2H_4} + \mathrm{O_2} &\rightarrow \mathrm{C_2H_3} + \mathrm{HO_2},\\
\mathrm{C_2H_4} + \mathrm{OH} &\rightarrow \mathrm{C_2H_3} + \mathrm{H_2O},\\
\mathrm{C_2H_4} + \mathrm{O} &\rightarrow q\mathrm{CH_3} + q\mathrm{CHO} + (1-q)\,\mathrm{CH_2CHO} + (1-q)\,\mathrm{H},\\
\mathrm{C_2H_4} + 2\mathrm{HO_2} &\rightarrow \mathrm{CH_3} + \mathrm{CO} + \mathrm{H_2O_2} + \mathrm{OH},\\
\mathrm{C_2H_4} + \mathrm{H} &\rightarrow r\mathrm{C_2H_3} + r\mathrm{H_2} + (1-r)\,\mathrm{C_2H_5},\\
\mathrm{C_2H_3} + \mathrm{O_2} &\rightarrow s\mathrm{CH_2O} + s\mathrm{CHO} + (1-s)\,\mathrm{CH_2CHO} + (1-s)\,\mathrm{O},\\
\mathrm{CH_3} + \mathrm{O_2} &\rightarrow \mathrm{CH_2O} + \mathrm{OH},\\
\mathrm{CH_2CHO} &\rightarrow \mathrm{CH_2CO} + \mathrm{H},\\
\mathrm{C_2H_5} + t\mathrm{O_2} &\rightarrow \mathrm{C_2H_4} + t\mathrm{HO_2} + (1-t)\,\mathrm{H},\\
\mathrm{CHO} + (1-u)\,\mathrm{O_2} &\rightarrow \mathrm{CO} + u\mathrm{H} + (1-u)\,\mathrm{HO_2}.
\end{aligned}
$$

Figure 5-4: Simplified ethylene-air mechanism[9]

For this proposed mechanism, each reaction can be treated as a differential equation relating the relative concentrations of each species by the law of mass action.

$$\omega = \frac{dn_i}{dt}/(\nu_i'' - \nu_i') \quad (5.3)$$

While a simplified mechanism can elucidate the concepts of finite rate chemistry, they are not always accurate in their prediction, and must be verified against experimental data and more advanced mechanisms for their validity [18]. Solving the system of coupled differential equations is a very computationally intensive task and falls outside the scope of this thesis. However, results from other research will be presented here to inform the kinetics of ethylene combustion. In one comprehensive study by Xu and Konnov, multiple ethylene-air mechanisms were tested against each other and experimental data[11]. It was found that their prediction for ignition delay time τ_i matched well with each other:

With this correlation, it is now possible to estimate chemical reaction time scales according to

$$\tau_i = Aexp\left(\frac{E}{RT}\right)[O_2]^a[C_2H_4]^b \quad (5.4)$$

where A is the reaction's rate constant, T is temperature, and E is the activation energy, all related by the Arrhenius equation and the concentrations of the reactants [17]. From this data one can observe that the ignition delay time of ethylene and air at conditions similar to a scramjet combustor are on order of 1ms - assuming combustion at 1200K and 3 atm. With this new information we can now better inform the heat release curve input into the model.

5.2.4 Modified Temperature Distribution

In order to more closely model the temperature distribution found in a scramjet combustor, a modified equation for robust heat deposition is borrowed from [3].

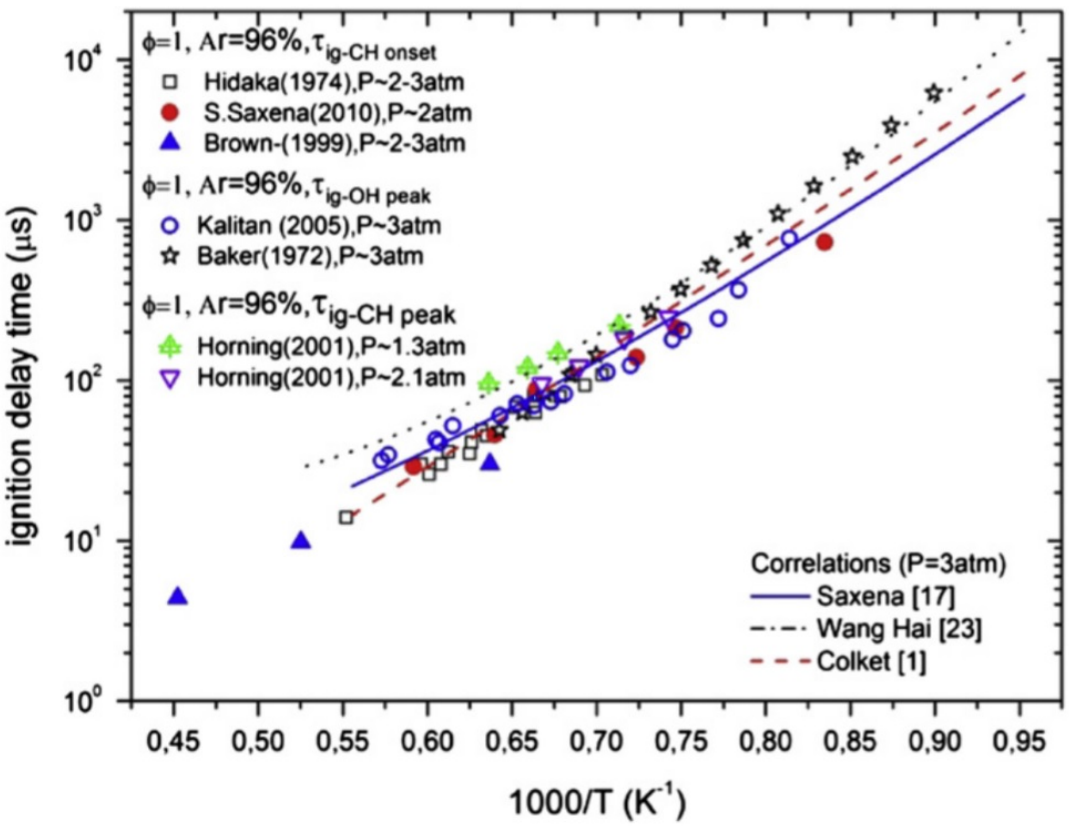

Figure 5-5: Ethylene ignition delay data at $\phi = 1$[11]

$$T_t = T_{t2} + (h_r f_s \phi \eta_c)/c_p \tag{5.5}$$

where η_c is a heat release efficiency according to

$$\eta_c = \eta_{ct}\left[\frac{\Theta X}{1 + (\Theta - 1)X}\right] \tag{5.6}$$

What is important about this result is that the fast kinetics of ethylene combustion result in a rapid release of heat as the flow proceeds down the combustor. While this is good for combustion efficiency, this make cause boundary layer separation in the isolator, which is a consideration designers will have to account for.

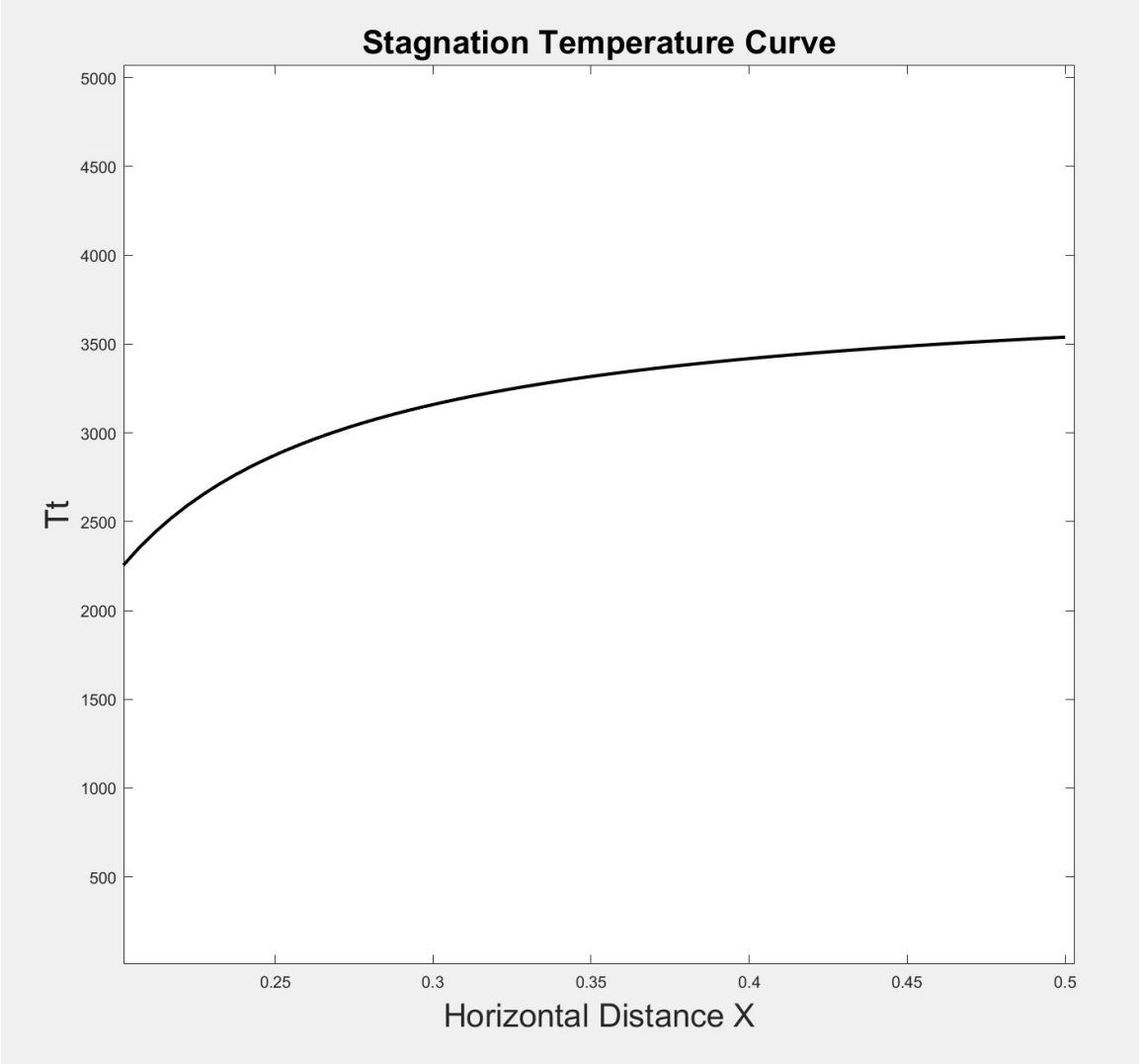

Figure 5-6: Sample stagnation temperature curve

5.3 Results

With this new knowledge, we would like to simulate a scramjet operating at a hypersonic flight number using ethylene fuel. The 1D model shall be able to predict, given reasonable input values, performance parameters as well as detailed explanations of flow physics within the isolator and combustor as far as a 1D model is capable. It is assumed that the conditions under which combustion occurs are met; namely, fuel and air have mixed sufficiently and the ignition and flame holding are steady. For a flight Mach number of 7 at an altitude of 20km, the following results are found:

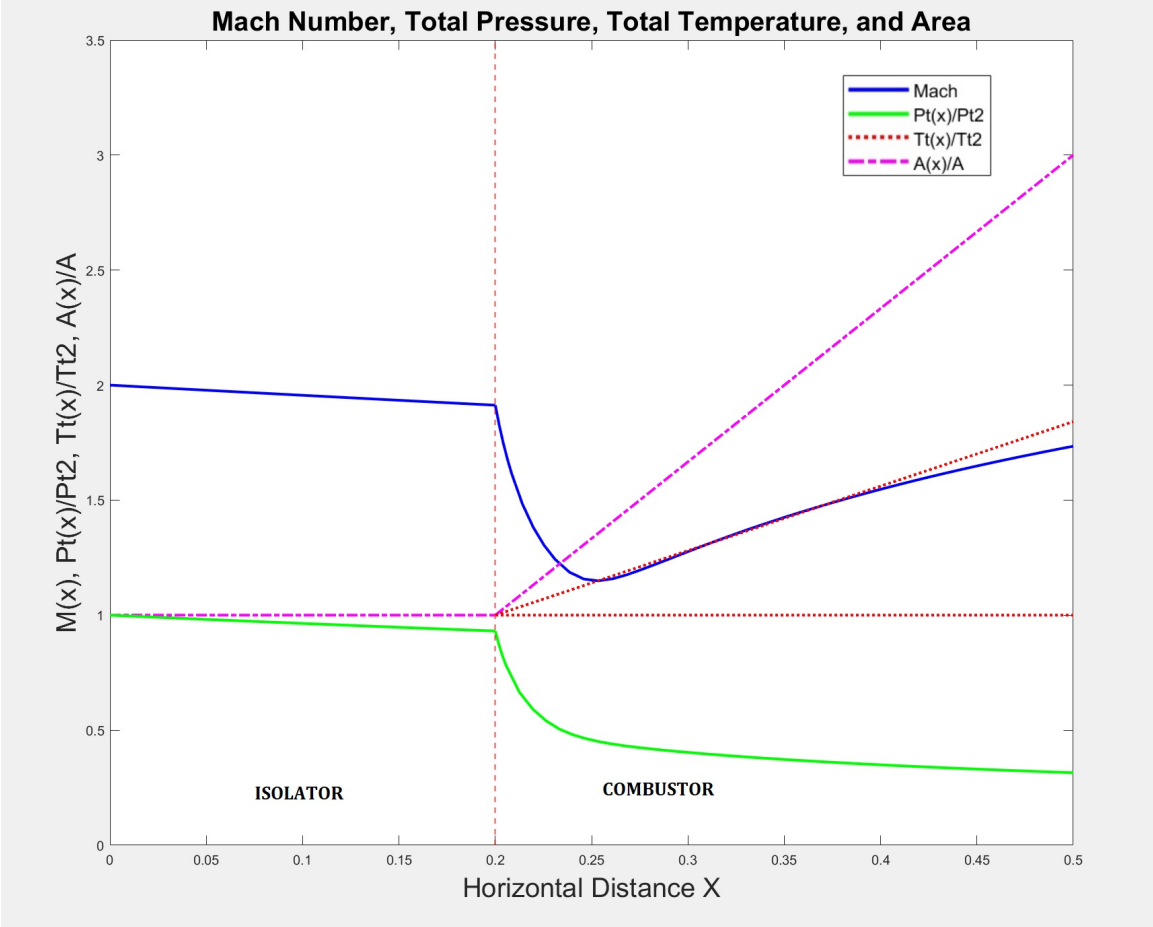

Figure 5-7: Isolator and combustor with non linear heat deposition

Here, a few physical insights can be found: supersonic combustion at Mach 2 causes significant stagnation pressure losses at nearly 60 percent, and due to the short ignition delay of ethylene τ_i, the heat release is rapid in comparison to flow through time, indicating $Da < 1$. Additionally, area scheduling must be more aggressive to prevent thermal choking, as it must increase from A to 3A along the combustor's span. We also see that the Mach number rapidly decreases, indicating a static pressure rise, which then starts to increase again due to expansion in the combustor.

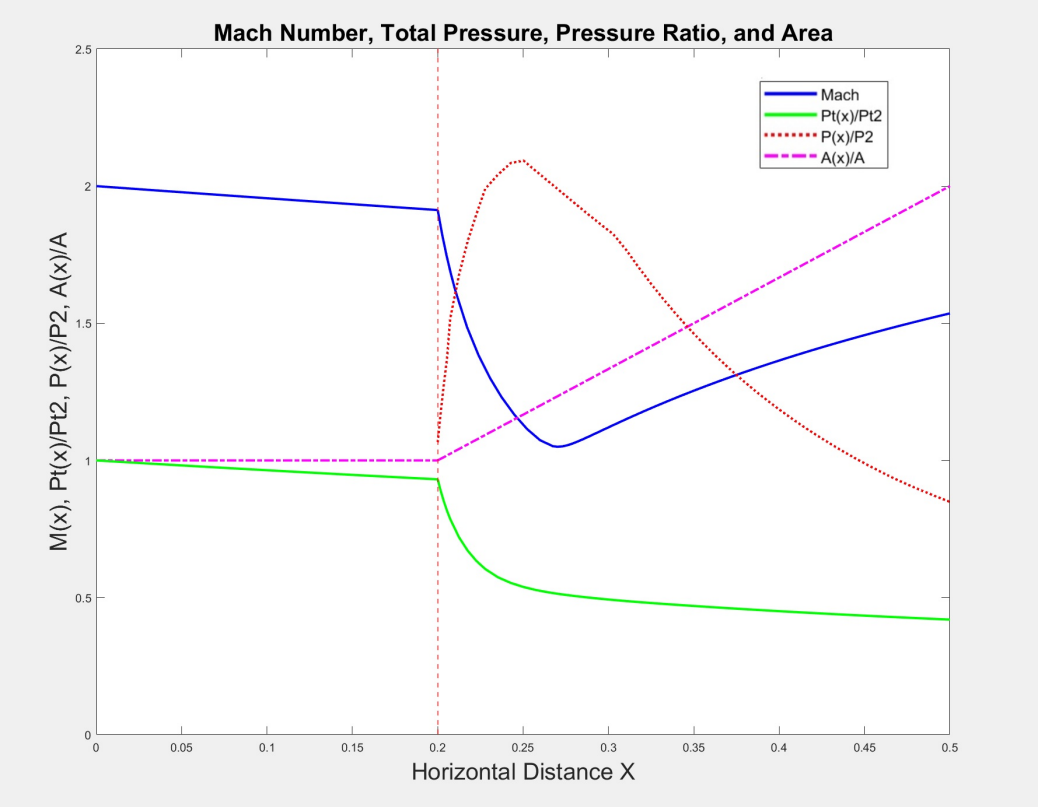

Figure 5-8: Isolator and combustor static pressure rise at $\phi = .5$

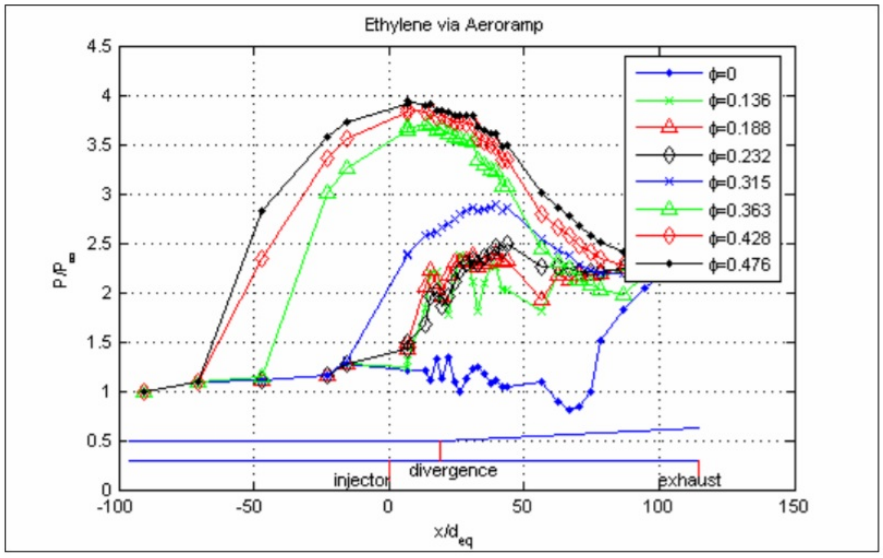

Figure 5-9: Pressure rise in experimental combustor at T = 1000K[12]

Here we see the trends of static pressure rise in a experimental combustor, and we can readily see that the trends are replicated by the 1D model. In order to

exactly mimic the numbers, however, detailed boundary conditions are required as input to the model. The results from the 1D model have the same exact trend but there is a discrepancy in terms of magnitude of pressure rise. This can be attributed to differences in flow area and entrance Mach number between the model and the experiment.

5.4 Conclusion

In this thesis, a 1D scramjet model with ethylene fuel was created. The model accurately predicts the stagnation and static quantities within a scramjet and can simulate the trends found in real life experiments. Specifically, using modified 1D compressible channel flow equations it can model both separated flow in an isolator as well as non linear heat deposition in a combustor.Additionally, it is capable of analyzing the scramjet as a whole as well as individual components. The 1D model gives significant physical insight to scramjet operation in the following ways, as it establishes qualitative trade offs that scramjet analysis necessitate:

1. Increasing flight Mach number M_0 and decreasing combustor inlet Mach number M_3 increases ratio M_0/M_3. which results in a higher thermal efficiency

2. Reducing M_3 also reduces stagnation pressure losses as combustion occurs, this is due to the dT_t/dM term scaling with $\gamma M^2/2$.

3. However, reducing M_3 can result in stagnation pressure losses in the inlet due to a reduction in kinetic energy efficiency, up to 50 percent for M = 10 and above.

4. Reducing M_3 can also result in boundary layer separation in the isolator due to higher static pressure rise in the combustor. This then results in a shock train and further unwanted stagnation pressure losses.

5. Lastly, reducing M_3 to unity will result in thermal choke due to sudden drop in the Mach number, but this can be counteracted by a careful area schedule of

dA/dx.

With the model readily capable of mimicking these qualitative trends, estimations for quantitative values of Mach number, pressure, etc. can be calculated with specified boundary conditions. It was a matter of design to leave most variables non dimensional as the emphasis is on physical insight as opposed to exact numeric values.

Improvements to the model can be made in the following ways:

1. Relaxing the assumption of adiabatic flow would allow the model to simulate heat transfer from the the fluid to the scramjet body

2. A more advanced kinetic model would give insight to the exact chemical structure of the flow as it proceeds along the combustor. One of the problems of supersonic combustion is dissociation, which chemical kinetics can model. Being that it has multiple species simultaneously reacting with each other, this would be an advanced combustor calculation well suited for the most in depth kinetic solvers available.

3. Currently modeling of separated flow in the isolator is manually setup by the user, however, using the separation criteria of Korkegi[19], a more advanced code could have an iterative setup which automatically calculates the separated flow.

Bibliography

[1] Kashkhan. Propulsion performance. Wikipedia, 2009.

[2] NASA. Rockwell x-30. Website, 2017.

[3] Michael Smart. Scramjet isolators. Technical report, University of Queensland.

[4] et al. Riggins, David. Thermodynamic analysis of dual-mode scramjet engine operation and performance. *AIAA*, 2005.

[5] Geometric altitude vs. temperature, pressure, density, and the speed of sound derived from the 1962 u.s. standard atmosphere. Technical report, 1962.

[6] D.M. Van Wie. *Scramjet Inlets*. Scramjet Propulsion (Progress in Astronautics and Aeronautics).

[7] Edward M. Greitzer and Choon S. Tan. *Internal Flow: Concepts and Applications*. Cambridge University Press, NY, NY, first edition, 2004.

[8] P. J. Waltrup and F.S. Billig. Prediction of precombustion wall pressure distributions in scramjet engines. *Journal of Spacecraft*, 1973.

[9] Corin Segal. *The Scramjet Engine: Processes and Characteristics*. Cambridge University Press, NY, NY, first edition, 10 August 2009.

[10] Michael Smart. Comparison between hydrogen and methane fuels in a 3-d scramjet at mach 8. Technical report, University of Queensland, 2016.

[11] Alexander A. Konnov Chaoqi Xu a, b. Validation and analysis of detailed kinetic models for ethylene combustion. *Journal of Energy*, 2011.

[12] Aristides M. Bonanos. *Scramjet Operability Range Studies of an Integrated Aerodynamic-Ramp-Injector/Plasma-Torch Igniter with Hydrogen and Hydrocarbon Fuels*. PhD dissertation, Virginia Polytechnic Institute, 2005.

[13] Kathleen Tran. One dimensional analysis program for scramjet and ramjet flowpaths. Master's thesis, virginia Polytechnic Institute, 2010.

[14] Sannu Mölder. The busemann air intake for hypersonic speeds. *intechOpen*, 2019.

[15] A.S. Shapiro. *The Dynamics and Thermodynamics of Compressible Fluid Flow.* John Wiley sons, New York.

[16] G. SULLINS and G. MCLAFFERTY. Experimental results of shock trains in rectangular ducts. *AIAA*, 1992.

[17] Rodger J. Biasca. Chemical kinetics of scramjet propulsion. Master's thesis, Massachusetts Institute of Technology, 1988.

[18] M. Ferrier A. Vincent-Randonnier Y. Moule V. Sabel'Nikov D. Scherrer, O. Dessornes. Research on supersonic combustion and scramjet combustors at onera. *AerospaceLab*, 2016.

[19] Korkegi R. H. Simple correlation for incipient turbulent boundary-layer separation due to a skewered shock wave. *AIAA*, 1973.